Petrogenesis and tectonic-magmatic context of emplacement of lepidolite and petalite pegmatites from the Fregeneda-Almendra field (Variscan Central Iberian Zone): clues from Nb-Ta-Sn oxide U-Pb geochronology and mineral geochemistry

Christophe Ballouard, Patrick Carr, Flore Parisot, Eric Gloaguen, Jérémie Melleton, Jean Cauzid, Andreï Lecomte, Olivier Rouer, Lise Salsi, Julien Mercadier

BSGF - Earth Sciences Bulletin 2024, 195, 3
© C. Ballouard *et al.*, Published by EDP Sciences 2024
https://doi.org/10.1051/bsgf/2023015

BSGF Earth Sciences Bulletin

Available online at:
www.bsgf.fr

Special Issue Some applications of LA-ICP-MS U-Pb geochronology: A tribute to Jean Louis Paquette Marc Poujol, Valérie Bosse and Dave Chew (Guest Editors)

OPEN ACCESS

Petrogenesis and tectonic-magmatic context of emplacement of lepidolite and petalite pegmatites from the Fregeneda-Almendra field (Variscan Central Iberian Zone): clues from Nb-Ta-Sn oxide U-Pb geochronology and mineral geochemistry

Christophe Ballouard[1,*], Patrick Carr[1], Flore Parisot[1], Éric Gloaguen[2,3], Jérémie Melleton[2], Jean Cauzid[1], Andreï Lecomte[1], Olivier Rouer[1], Lise Salsi[1] and Julien Mercadier[1]

[1] Georessources, UMR 7359, Université de Lorraine, CNRS, Nancy 54000, France
[2] BRGM, F-45060 Orléans, France
[3] ISTO, UMR 7327, Université d'Orléans, CNRS, BRGM, F-45071 Orléans, France

Received: 24 June 2023 / Accepted: 3 October 2023 / Publishing online: 10 January 2024

Abstract – The Fregeneda-Almendra pegmatite field of the Iberian Massif represents a typical expression of peraluminous rare-metal magmatism that occurred over western Europe at the end of the Variscan orogeny. It is the host for two main types of Li-mineralized intrusions, identified at the scale of the Variscan belt, including petalite- or spodumene-rich pegmatites, as well as Li-mica-rich pegmatites, for which the origin of mineralogical-chemical differences is not yet understood. Here, we provide cassiterite and columbite-group mineral (CGM) U-Pb ages along with oxide, mica and phosphate mineral compositions for Li-pegmatites from the Fregeneda-Almendra field in order to assess their petrogenesis and tectonic-magmatic context of emplacement. U-Pb geochronology indicates that petalite-rich and Li-mica-rich pegmatites were mostly emplaced sub-synchronously from 315 ± 6 to 308 ± 6 Ma, during strike-slip deformation and granitic magmatism within an anatectic dome bounding the pegmatite field. U-Pb data and pegmatite geographic zonation suggest that Li-pegmatites were sourced from buried equivalents of leucogranites and migmatites from the dome. Li-pegmatites experienced a complex crystallization including K-feldspar, petalite, topaz, Nb-Ta-Fe-Mn-rich cassiterite, amblygonite-group minerals (AGM) and CGM as early magmatic phases, followed by lepidolite for Li-mica-rich pegmatites. At the magmatic-hydrothermal transition, notably leading to the formation of Nb-Ta-Mn-Fe-poor cassiterite hosting CGM inclusions, earlier minerals were resorbed by muscovite and albite. A later F-rich hydrothermalism is locally reflected by zinnwaldite overgrowths on muscovite. Cassiterite, CGM and micas from petalite-rich pegmatites show lower Mn/Fe ratios and higher Ti contents, along with lower Zr-Ga contents for cassiterite, than that from Li-mica-rich pegmatites. Such behavior is consistent with a magmatic differentiation process whereby Ti content decreased and the degree of Mn-Fe geochemical fractionation and solubilities of Ga and Zr increased in the melts, possibly in relation with high fluorine activity. In Li-mica-rich pegmatites, AGM equilibrated with a melt with up to 2 wt% F, similar to that in equilibrium with lepidolite (1–3 wt%). In petalite-rich pegmatites, the relatively high F concentration of the melts equilibrated with AGM ($\leq$ 1.5 wt% F) contrasts with the liquid equilibrated with muscovite ($<$ 0.5 wt% F). This can be accounted for by muscovite crystallization after the exsolution of a F-rich aqueous phase at the magmatic-hydrothermal transition. Relatively similar F contents in the initial melts of petalite- and Li-mica-rich pegmatites support the hypothesis that the stability of lepidolite does not only involve high F but also a low H_2O/F activity ratio. For the Fregeneda-Almendra Li-mica-rich pegmatites, this could be explained by a decrease of melt H_2O solubility due to a relatively low pressure of emplacement.

Keywords: Lepidolite and petalite pegmatites / Variscan Iberian Massif / strike-slip tectonics / cassiterite / columbite-group minerals / U-Pb geochronology

*e-mail: christophe.ballouard@univ-lorraine.fr

Résumé – Pétrogenèse et contexte tectonique-magmatique de mise en place des pegmatites à pétalite et lépidolite de la ceinture de la Fregeneda-Almendra (Zone centrale ibérique de la Chaîne varisque) : aperçu de la cristallochimie et de la géochronologie U-Pb des oxydes de Nb-Ta-Sn. Le champ de pegmatites de la Fregeneda-Almendra représente une expression typique du magmatisme peralumineux à métaux rares de la fin de l'orogenèse varisque. Il est l'hôte de deux principaux types d'intrusions minéralisées en Li incluant des pegmatites à pétalite ou spodumène, et à micas lithinifères (mica-Li), dont l'origine des différences cristallochimiques est mal comprise. Nous fournissons ici des âges U-Pb sur cassitérite et minéraux du groupe de la colombite (coltan) ainsi que la composition des oxydes, micas et phosphates de ces pegmatites afin d'évaluer leur pétrogenèse et leur contexte de mise en place. La géochronologie U-Pb indique que les pegmatites à pétalite et à mica-Li se sont mises en place de manière sub-synchrone de 315 ± 6 à 308 ± 6 Ma, lors d'une déformation en décrochement et du magmatisme granitique dans un dôme anatectique délimitant le champ de pegmatites. Les âges et la zonation géographique des pegmatites suggèrent que les leucogranites et migmatites du dôme représentent des équivalents de leur source. Les pegmatites à Li enregistrent une cristallisation complexe comprenant : feldspath-K, pétalite, topaze, cassitérite riche en Nb-Ta-Fe-Mn, minéraux du groupe de l'amblygonite (MGA) et coltans comme phases magmatiques précoces, suivies du lépidolite pour les pegmatites à mica-Li. À la transition magmatique-hydrothermale, conduisant notamment à la formation de cassitérite pauvre en Nb-Ta-Mn-Fe, les minéraux précoces ont été résorbés par la muscovite et l'albite. Un hydrothermalisme tardif riche en F est reflété par des surcroissances de zinnwaldite sur la muscovite. Les oxydes et les micas des pegmatites à pétalite présentent des rapports Mn/Fe et des teneurs en Zr et Ga plus faibles ainsi que des teneurs en Ti plus élevées que ceux des pegmatites à mica-Li. Ceci est cohérent avec un processus de différenciation magmatique durant lequel la teneur en Ti a diminué, et le fractionnement de Mn-Fe et les solubilités de Zr et Ga ont augmenté dans le liquide, possiblement en relation avec une augmentation de l'activité en F. Dans les pegmatites à mica-Li, les MGA étaient équilibrés avec un liquide silicaté contenant jusqu'à 2%pds de F, similaire à celui en équilibre avec le lépidolite (1–3%pds). Dans celles à pétalite, la concentration en F relativement élevée du liquide équilibré avec l'AGM ($\leq$ 1,5%pds F) contraste avec celui équilibré avec la muscovite ($<$ 0,5%pds F). Ceci peut s'expliquer par la cristallisation de la muscovite après l'exsolution d'une phase aqueuse riche en F. Des teneurs en F relativement similaires dans les liquides initiaux des pegmatites à pétalite et mica-Li suggèrent que la stabilité du lépidolite n'implique pas seulement une activité élevée en F mais aussi une faible activité en H_2O relative au F. Pour les pegmatites à mica-Li de la Fregeneda-Almendra, ceci pourrait s'expliquer par une diminution de la solubilité de l'H_2O dans le liquide parent due à une pression de mise en place relativement faible.

Mots clés : Pegmatites à pétalite et lépidolite / Massif ibérique de la chaîne varisque / tectonique décrochante / cassitérite / minéraux du groupe de la colombite / géochronologie U-Pb

1 Introduction

Lithium has become a strategic commodity as it represents a key component for green energy-storage devices, such as Li-ion batteries. In Europe, significant "hard-rock" Li resources are associated with peraluminous high phosphorous rare-metal granites (Linnen and Cuney, 2005) and LCT-type pegmatites (enriched in Li-Cs-Ta, Černý and Ercit, 2005) from the Variscan belt (Gourcerol *et al.*, 2019) (Fig. 1). Mineralization of Li-bearing aluminosilicate phases such as spodumene, petalite or Li-micas (*e.g.*, micas from the lepidolite series) along with Li-Al-phosphates (amblygonite-group minerals) typically occur disseminated within those intrusions. Moreover, rare-metal granites and pegmatites are commonly enriched in other strategic metals such as Sn, Ta and Nb generally hosted in oxide minerals including cassiterite, columbite-group and pyrochlore-group minerals (Linnen *et al.*, 2012).

Peraluminous rare-metal pegmatites and granites (RMPGs) are related to crustal melting in late-orogenic setting and can reach metal (*e.g.*, Li, Be, Ta, Nb, Sn, Cs) and halogen (F) concentrations that are up to three orders of magnitude higher than bulk upper crust and common peraluminous granites (Černý *et al.*, 1985; Linnen and Cuney, 2005; Romer and Pichavant, 2021). Magmatic-hydrothermal processes including silicate melt-hydrosaline melt or melt-fluid immiscibility and alkali metasomatism can lead to significant element mobility and re-concentration at the end of magma crystallization (Kaeter *et al.*, 2018; Müller *et al.*, 2018; Ballouard *et al.*, 2020a, 2020b). However, the occurrences of volcanic to sub-volcanic equivalents of RMPGs (Pichavant *et al.*, 1987; Raimbault and Burnol, 1998) as well as experiments (Pichavant, 2022) suggest that their metal enrichment occurred dominantly at the magmatic stage. Rare-metal-enriched dykes or stocks, especially LCT pegmatites, commonly cluster in fields or belts with a lateral extent of ten's kilometers or more and commonly define a geographic and geochemical zonation around peraluminous plutons (Černý, 1991). As such, pegmatites from the same field are commonly interpreted as coeval, cogenetic and issued from variable degrees of fractional crystallization of the same parent pluton (Černý and Ercit, 2005; Hulsbosch *et al.*, 2014; London, 2018). However, spatially associated granites and pegmatites can feature distinct ages (Melleton *et al.*, 2012, 2022; Müller *et al.*, 2017) or geochemical and isotopic signatures (Antunes *et al.*, 2013; Deveaud *et al.*, 2015; Villaros and Pichavant, 2019) incompatible with parent-daughter relationships and suggesting variable partial melting conditions or source

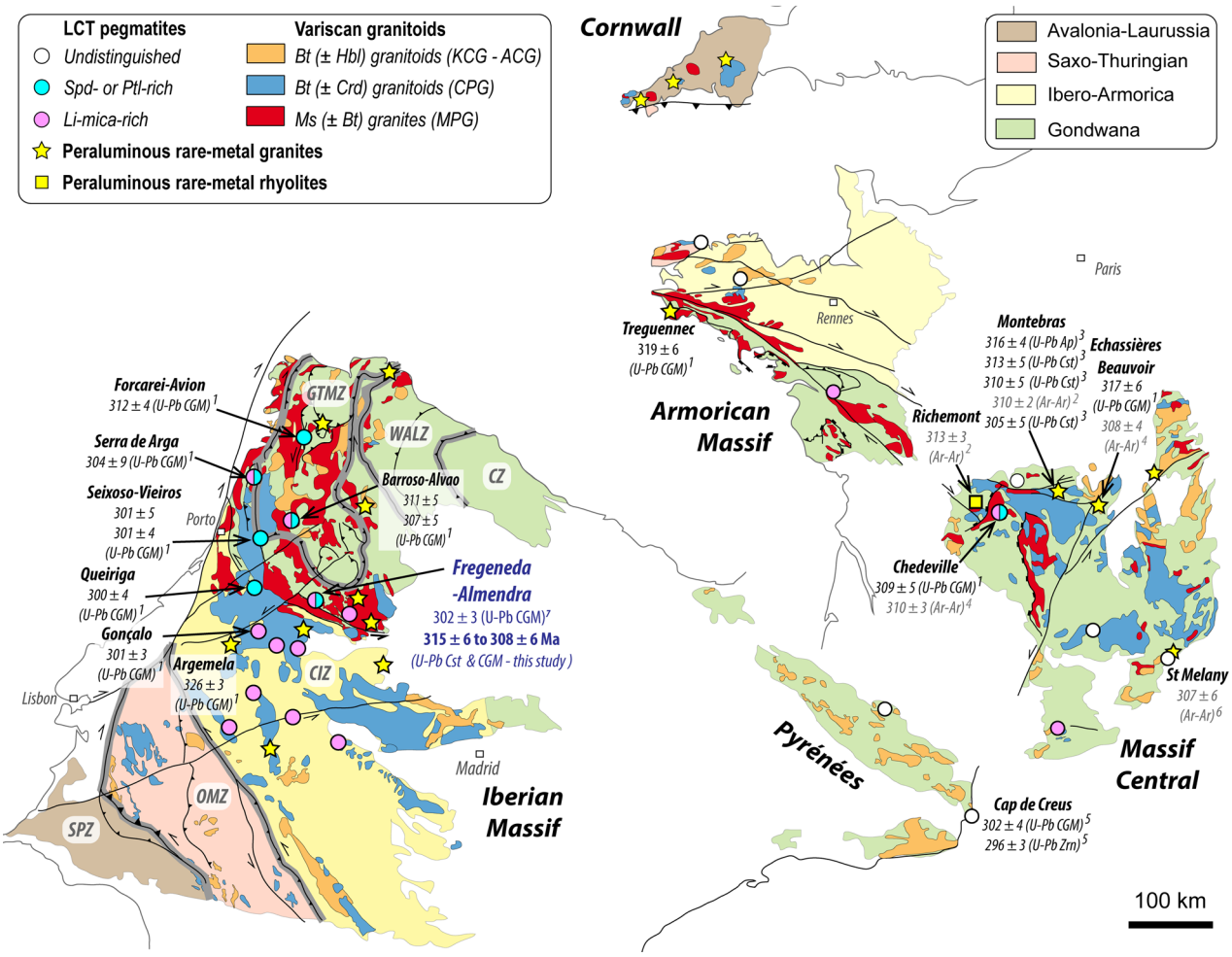

Fig. 1. Simplified geological map of the west European Variscan belt showing the main geological terranes (adapted from Ballèvre *et al.*, 2009, 2014; Ballèvre, 2016), the location of peraluminous rare-metal granites and LCT (Li-Cs-Ta) pegmatites, including petalite (Ptl)-spodumene (Spd)-rich and Li-mica-rich types (Roda-Robles *et al.*, 2018; Gourcerol *et al.*, 2019), as well as Variscan granitoids (Chantraine *et al.*, 2003; Rodríguez Fernández and Oliveira, 2014; Simons *et al.*, 2016; Ribeiro *et al.*, 2019). The ages of rare-metal granites and pegmatites provided in Ma with 2σ error are from 1: Gourcerol *et al.* (2019), Melleton *et al.* (2022) ; 2: Cuney *et al.* (2002); 3: Marcoux *et al.* (2021); 4: Cheilletz *et al.* (1992); 5: Van Lichtervelde *et al.* (2017); 6: Chauvet *et al.* (2012); 7: Roda-Robles *et al.* (2023). Dating methods include U-Pb on columbite-group mineral (CGM), cassiterite (Cst), apatite (Ap) and zircon (Zrn) as well as muscovite or Li-mica $^{40}Ar/^{39}Ar$ (Ar-Ar) geochronology. Granitoid typology is from Barbarin (1999). Other abrreviations: MPG: muscovite-bearing peraluminous granite, CPG: cordierite-bearing peraluminous granite, KCG: K-rich K-feldspar porphyritic calc-alkaline granitoid, ACG: amphibole-rich calc-alkaline granitoid, SPZ: South Portuguese Zone, OMZ: Ossa Morena Zone, CIZ: Central Iberian Zone, GTMZ: Galicia Trás Os Montes Zone, WALZ: West Asturian-Leonese Zone, CZ: Cantabrian Zone. Iberian zone boundaries are shown in grey.

heterogeneities. On this basis, some studies have suggested that some LCT pegmatites are directly produced by small degree of partial melting of metasedimentary protoliths variably enriched in rare-metal and fluxing elements such as Li and F (Stewart, 1978; Shaw *et al.*, 2016; Konzett *et al.*, 2018b, 2018a; Gourcerol *et al.*, 2019; Bonzi *et al.*, 2021). Alternative models combining favorable partial melting conditions of rare-metal fertile protoliths followed by magmatic differentiation have also been proposed for the formation of LCT pegmatite deposits (Knoll *et al.*, 2018, 2023; Ballouard *et al.*, 2020a, Ballouard *et al.*, 2023). Overall, no general consensus exists regarding the key processes controlling the genesis of RMPGs.

Moreover, the extraction and transport of rare-metal-enriched silicic magmas from their migmatitic or granitic sources to upper crustal levels are commonly seen as being the results of favorable tectonic conditions with their emplacement intimately controlled by deformation structures (Araújo *et al.*, 2001; Demartis *et al.*, 2011; Deveaud *et al.*, 2013; Gourcerol *et al.*, 2019; Ballouard *et al.*, 2020a; Michaud *et al.*, 2020). However, the few robust geochronological data available for RMPGs is a strong limitation for our understanding of their tectonic-magmatic contexts of formation. Traditional refractory phases with high-closure temperature U-Pb systems such as zircon are commonly rare, or when present, highly metamict in these geological environments.

The Fregeneda-Almendra (FA) pegmatite field, located in the Central Iberian Zone (CIZ) of the Variscan Iberian Massif at the boundary between Spain and Portugal, is a typical expression of peraluminous rare-metal magmatism that occurred at the end of the Variscan orogeny in western Europe (Roda-Robles *et al.*, 1999, 2023; Vieira *et al.*, 2011; Errandonea-Martin *et al.*, 2022) (Fig. 1). This field hosts the two main types of LCT pegmatites identified in the Iberian Massif, including (i) spodumene- or petalite-rich, as well as (ii) Li-mica-rich pegmatites (Roda-Robles *et al.*, 2016, 2018, 2023). If the stability of spodumene over petalite is known to be mostly pressure- and temperature-dependent (London 1984, 2018), few constraints exist on the conditions of crystallization of Li-micas such as lepidolite over other Li-aluminosilicates, except for the requirement of a Li-F-rich peraluminous melt (London and Burt, 1982) with possibly high alkali-fluorine salinity (Wise *et al.*, 2012). Previous studies on Iberian pegmatites including the FA pegmatite field have suggested based on whole-rock (Roda-Robles *et al.*, 2018, 2023), mica (Vieira *et al.*, 2011) and phosphate mineral (Roda-Robles *et al.*, 2010) compositions that Li-mica-rich pegmatites represent the most evolved residual melts of a fractional crystallization series including as more primitive members the petalite- and spodumene-rich pegmatites. However, the cogenetic character of such Li-pegmatites was questioned in a similar pegmatite field from Iberia (*i.e.*, Barosso-Alvao) based on columbite-group mineral (CGM) geochemistry (Martins *et al.*, 2011).

The pegmatites of the FA field were emplaced within a belt of metasedimentary rocks in contact to the south with a major anatectic dome and bounded by sinistral strike-slip shear zones; the dome mostly consists of syntectonic two-mica-bearing leucogranites and migmatites, referred to as the Figueira de Castelo Rodriguo-Lumbrales (FCL) complex (Díez Fernández and Pereira, 2016; Ferreira *et al.*, 2019, 2020, 2022) (Fig. 2a). The pegmatites tend to define a zonal distribution around the FCL complex with a northward increase of Li-fertility, roughly perpendicular to metamorphic isograds, from barren pegmatites close to or within the anatectic complex to petalite-rich pegmatites, spodumene-rich and Li-mica-rich pegmatites in lower grade metasedimentary rocks (Roda-Robles *et al.*, 1999; Vieira *et al.*, 2011) (Fig. 2b). However, available muscovite and Li-mica $^{40}Ar/^{39}Ar$ geochronology of pegmatites from the FA field yielded ages from ca. 305 to 295 Ma (Roda-Robles *et al.*, 2009, 2023). These Ar-Ar ages, as well as one U-Pb age of 302 ± 3 Ma obtained on a CGM crystal from a Li-mica-rich pegmatite (Roda-Robles *et al.*, 2023), are significantly younger than the crystallization age of the main leucogranite intrusions from the FCL complex (ca. 319-311 Ma, zircon U-Pb; Ferreira *et al.*, 2019), as well as U-Pb zircon ages of associated migmatites (ca. 344–315 Ma; Ferreira *et al.*, 2020, 2022). Roda-Robles *et al.* (2009, 2023), thus, concluded for an absence of genetic connection between leucogranites from the FCL complex and Li-mineralized pegmatites from the FA field, and proposed a genetic link with non-outcropping late- to post-orogenic granites. However, such disconnection is strange considering the apparent spatial relationship between the FCL dome and the pegmatites (Fig. 2).

In this study, we use a new approach based on cassiterite U-Pb geochronology, coupled with CGM U-Pb dating along with oxide mineral, mica and phosphate geochemical compositions, on Li-mica- and petalite-rich pegmatites from the FA field. Our goal is to precisely determine the timing of emplacement of Li-pegmatites within the regional tectonic-magmatic framework, and to better decipher the petrogenetic processes involved during the crystallization of rare-metal-bearing mineral phases including Li-aluminosilicates.

2 Geological setting

2.1 The Central Iberian Zone

The Iberian Massif represents the south-western part of the European Variscan belt, a Paleozoic orogen resulting from the collision of supercontinents Laurussia and Gondwana, and involving several micro-continental blocks such as Iberia and Armorica (Matte, 1991; Kroner and Romer, 2013; Ballèvre *et al.*, 2014; Martínez Catalán *et al.*, 2021) (Fig. 1). The CIZ of the Iberian Massif largely consists of Precambrian to Cambrian metapelites and metagraywackes (the Schist-Graywacke Complex), overlain by Ordovician quartzites and intruded by voluminous Carboniferous to Permian granitoids, as well as Cambro-Ordovician igneous rocks (Dallmeyer and Garcia, 2012; García-Arias *et al.*, 2018). Three main deformation events were recognized in the Iberian Zone including (i) collision-related thrusting and folding during Barrovian metamorphism between ca. 360 and 335 Ma (D1), (ii) crustal extension accommodated by low-dipping extensional shear zones associated with low-pressure high-temperature metamorphism from ca. 335 to 320 Ma (D2), and (iii) strike-slip tectonics along vertical shear zones associated with upright folding between ca. 320 and 295 Ma (D3) before and until the final closure of the Ibero-Armorican arc (Dallmeyer *et al.*, 1997; Gutiérrez-Alonso *et al.*, 2011; Martínez Catalán *et al.*, 2014, 2021; Díez Fernández and Pereira, 2016; Dias da Silva *et al.*, 2017, Pereira *et al.*, 2017). Within the D3 event, Díez Fernández and Pereira (2016, 2017) suggested the existence of three distinct episodes of strike-slip deformations in Iberia occurring at ca. 317-311 Ma, 311-304 Ma and 304-295 Ma.

Voluminous granitoid magmatism in NW-Iberia occurred from ca. 345 to 285 Ma (Ábalos *et al.*, 2002; Gutiérrez-Alonso *et al.*, 2011, 2018; Martínez Catalán *et al.*, 2014, 2021). Granitoids can be classified as three main groups, including (i) syn-D3 highly peraluminous two-mica- or muscovite-bearing granites and leucogranites, (ii) late-D3 peraluminous biotite-bearing granites locally hosting cordierite, as well as (iii) pre-D3 and late-D3 generations of metaluminous to slightly peraluminous biotite ± amphibole-bearing granodiorites and granites (Ribeiro *et al.*, 2019). Those three granitoid types globally correspond to the muscovite-bearing peraluminous granites (MPG), cordierite-bearing peraluminous granites (CPG) and K-rich K-feldspar porphyritic calc-alkaline granitoids (KCG) of the general classification of Barbarin (1999) used in the map of Figure 1.

Despite their low volume compared to common granitoids, peraluminous Li-aplites or Li-pegmatites, hosting spodumene, petalite, Li-micas and/or Li-phosphates along with Sn-Nb-Ta oxide minerals, are widespread both in the Galicia-Trás-os-Montes and Central Iberian zones (Neiva and Ramos, 2010; Roda-Robles *et al.*, 2016, 2018) (Fig. 1). They were mostly emplaced during D3-related tectonics from ca. 315 to 300 Ma

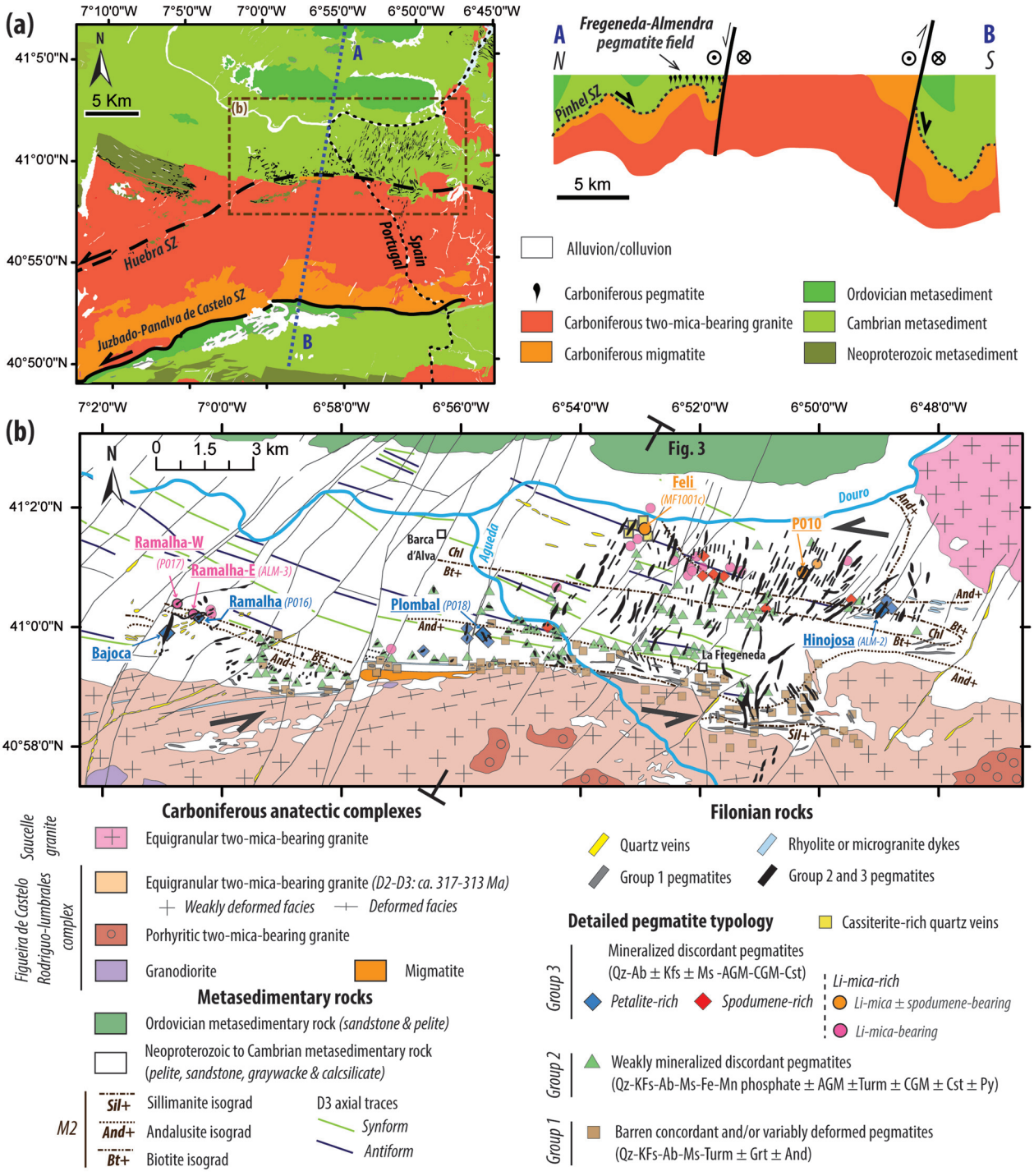

Fig. 2. Simplified geological map of the (a) Figueira de Castelo Rodriguo-Lumbrales anatectic complex and (b) Fregeneda-Almendra pegmatite field. Maps simplified from Ferreira *et al.* (2019), Díez Fernández and Pereira (2016) and 1: 50.000 geological maps of Portugal and Spain (Ferreira da Silva *et al.*, 1990b, 1990a; Villar *et al.*, 1990; Diez Montes *et al.*, 1991) with metamorphic isograds and detailed pegmatite typology from Vieira *et al.* (2011). The schematic A-B cross section in (a) was adapted from Díez Fernández and Pereira (2016). Mineral abbreviation from Whitney and Evans (2010); other abbreviations: CGM: columbite-group mineral; AGM: amblygonite-group mineral; SZ: shear zone.

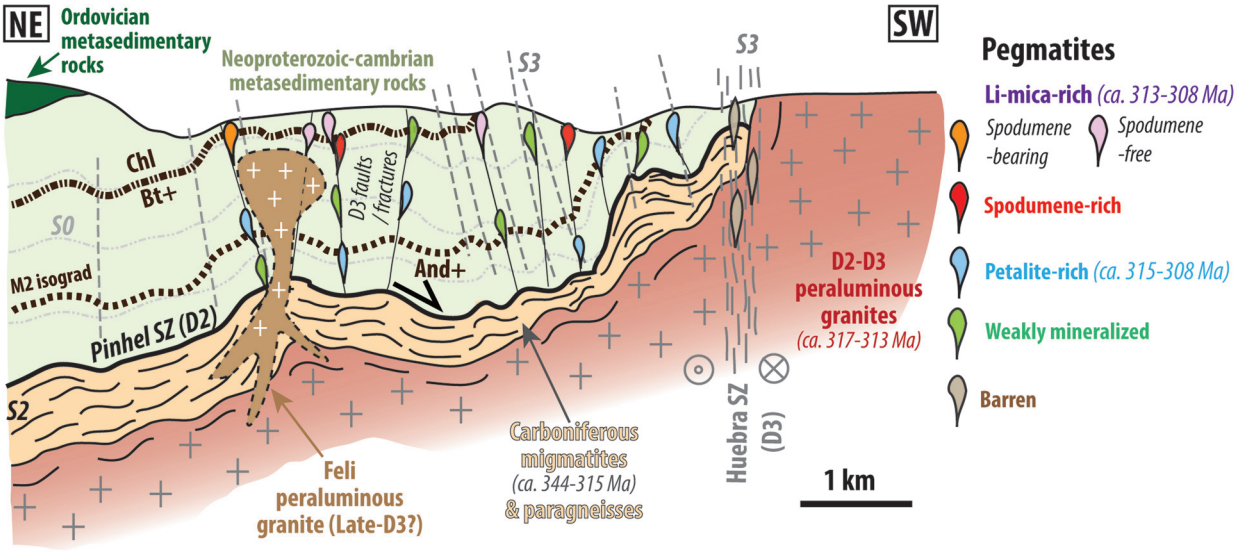

Fig. 3. Schematic cross section adapted from Díez Fernández and Pereira (2016, their Fig. 4d) illustrating the tectonic-magmatic context of emplacement of Fregeneda-Almendra pegmatites to the north of the FCL anatectic complex. The location of the cross section is indicated in Fig. 2b. High temperature-low pressure metamorphism-related M2 isograds (Carnicero, 1982; Vieira *et al.*, 2011) were drawn parallel to the D2 Pinhel shear zone (SZ). The size of the pegmatites is not to scale. The ages of Li-pegmatites are from this study and the ages of migmatites and granites are from Ferreira *et al.* (2019, 2022).

(U-Pb on CGM; Melleton *et al.*, 2022). Roda-Robles *et al.* (2018) proposed, on the basis of geochemical similarities, a genetic relationship between Li-pegmatites and highly peraluminous P-rich granite plutons. They distinguished two types of fertile granites including a S1-type series corresponding to two-mica-bearing leucogranites or MPG and a S2-series representing the most peraluminous terms of biotite ± cordierite-bearing granites or CPG.

2.2 The Figueira de Castelo Rodriguo-Lumbrales anatectic complex and associated Fregeneda-Almendra pegmatite field

The Figueira de Castelo Rodriguo-Lumbrales (FCL) anatectic complex is a more than 50 km long E-W to NE-SW oriented dome-like structure separated from lower grade metasedimentary rocks by two D3 sinistral shear zones including the Huebra shear zone to the north and Juzbado–Penalva do Castelo shear zone to the south (Fig. 2a). The two-mica-bearing peraluminous leucogranites are locally deformed and bear a roughly E-W oriented S3 sub-vertical foliation along the northern and southern edges of the FCL complex (Díez Fernández and Pereira, 2016). Most leucogranites were emplaced between 317 ± 2 and 313 ± 2 Ma (U-Pb zircon), and a late-D3 magmatic pulse marked by the emplacement of a muscovite-rich leucogranite intrusion occurred between 308 ± 3 Ma (Díez Fernández and Pereira, 2017) and 300 ± 2 Ma (Ferreira *et al.*, 2019). The beginning of emplacement of leucogranites at ca. 319-317 Ma was interpreted to mark the evolution from D2-related extension to D3-transpression, and thus a transition from vertical to horizontal shortening (Díez Fernández and Pereira, 2016). Ferreira *et al.* (2020) describe gradual transition from metatexites, diatexites, to syn-D3-leucogranites within the FCL complex, with peak low pressure-high temperature metamorphic conditions for calc-silicate rocks interlayered with metapelites of 760 ± 50 °C and 5.0 ± 1.0 kbar (Pereira *et al.*, 2017). U-Pb zircon ages of diatexites and metatexites from the FCL complex overlap with that of leucogranites and range from 344 ± 3 to 315 ± 1 Ma with peak metamorphism estimated at 317 ± 2 Ma (Ferreira *et al.*, 2022). Carboniferous migmatites and leucogranites from the FCL complex are separated from the overlying lower grade Neoproterozoic to Cambrian metasedimentary rocks by the Pinhel shear zone, a D2 extensional structure that was folded during D3 tectonics and eventually localized strike-slip shear zones such as the Huebra structure (Díez Fernández and Pereira, 2016) (Fig. 2a). The overlying metasedimentary envelope located to the north and south of the FCL complex was uprightly folded in relationship with both D1 and D3 deformations, and the core of major E-W oriented synclines is marked by the occurrence of Ordovician quartzites (Díez Fernández and Pereira, 2016).

The ~20 km long and up to 6 km wide Fregeneneda-Almendra pegmatite field occupies a roughly E-W oriented belt of Neoproterozoic to Cambrian metasedimentary rocks (Schist-Graywacke Complex) located to the north of the FCL complex and to the south-west of the two-mica leucogranite of Saucelle (López Plaza *et al.*, 1982; Villar *et al.*, 1990; Ferreira da Silva and Luisa Ribeiro, 1994; Roda-Robles *et al.*, 1999, 2023; Vieira *et al.*, 2011) (Fig. 2b). The supracrustal rocks mostly consist of metapelites, metagraywackes and quartzites with minor calc-silicate rocks. The roughly E-W-oriented sedimentary layering (S0) of metasedimentary rocks was affected by D1 and D3 folds with globally WNW-ESE oriented axes (Figs. 2b and 3), and S1 and S3 fabrics typically host a M1-M3-related greenschist-facies mineral assemblage (Díez Fernández and Pereira, 2016). The core of the main syncline structure occurring to the north of the FA field is filled by Paleozoic metasedimentary rocks. This suggests that the

sedimentary series was not overturned and that the thickness of the metasedimentary envelope increases toward the north (*i.e.*, a northward deepening of the D2 Pinhel extensional shear zone, bounding migmatites and leucogranites) (Díez Fernández and Pereira, 2016) (Figs. 2b and 3). Metamorphic isograds in metasedimentary rocks were interpreted as striking perpendicular to the contact with the FCL by Dias da Silva (2013). However, several studies have shown that the metamorphic grade of metasedimentary rocks increases toward the south and that the variably folded metamorphic isograds are oriented roughly parallel to the contact with the FCL complex (Carnicero, 1982; Ferreira da Silva *et al.*, 1990b, 1990a; Vieira, 2010) (Figs. 2b and 3). Index minerals defining those isograds evolve from (i) chlorite, (ii) biotite, (iii) andalusite ± cordierite to (iv) sillimanite toward the south and define a typical sequence of low pressure – high temperature metamorphism (Carnicero, 1982). Those M2-related index minerals are characteristic of S2 fabrics that developed in relation with deep crust exhumation, migmatization and leucogranitic magmatism during regional extension (Díez Fernández and Pereira, 2016).

Minor pegmatites were emplaced within leucogranites of the FCL and the majority was emplaced within Neoproterozoic to Cambrian metasedimentary rocks. Three main groups of pegmatites, along with ten subtypes, were defined in the FA pegmatite field (see Vieira *et al.,* 2011 and Roda-Robles *et al.,* 2023 for more detailed descriptions) (Fig. 2b). Group 1, including four subtypes (*i.e.*, T1-4), consists of intra- to peri-granitic barren pegmatite dykes bearing quartz, feldspar, muscovite, tourmaline ± andalusite ± garnet. They are commonly deformed and generally strike parallel to the roughly E-W oriented S3 foliation within the metasedimentary rocks and the leucogranites. Group 2 and Group 3 pegmatite dykes are generally sub-vertical and mainly crosscut the foliations of metasedimentary rocks with an NNE-SSW to NE-SW orientation, although their orientation and dip angles are locally variable, in particular close by the FCL complex (Figs. 2b and 4a) (Villar *et al.*, 1990). Group 2 weakly-mineralized pegmatites (T5-6) are characterized by the presence of Fe-Mn phosphates along with amblygonite-group minerals (AGM; [Li,Na)Al(PO_4)(F,OH)]), and variable proportion of columbite-group minerals (CGM) and cassiterite. Group 3 pegmatites also host AGM and are characterized by the presence Li-bearing aluminosilicates and a higher amount of cassiterite and CGM (Fig. 4). Vieira *et al.* (2011) identified four subtypes of Li-pegmatites (*i.e.*, Group 3) corresponding to petalite-rich (T7, Fig. 4a, b, c), spodumene-rich (± petalite-bearing) (T8), Li-mica-rich and spodumene-bearing (T9), and Li-mica-rich and spodumene-free (T10) (Fig. 4d, e, f) pegmatites. Those Li-pegmatite subtypes (T7 to T10) were interpreted as defining a progressive fractional crystallization series, with Group 2 weakly mineralized pegmatites as the least evolved members (Roda-Robles *et al.,* 2010, 2023; Vieira *et al.,* 2011). The degree of host-rock M2 metamorphism, defined by the presence of index minerals, seems to exert a primary control over the Li-pegmatite subtypes; petalite-rich pegmatites (T7) were mostly emplaced within the andalusite to biotite zones, whereas spodumene-rich pegmatites (T8) and Li-mica-rich ± spodumene-bearing pegmatites (T9-10) were dominantly emplaced in lower grade metasedimentary rocks within the biotite to chlorite zones (Vieira *et al.,* 2011) (Figs. 2b and 3). Moreover, a particular type of cassiterite-rich quartz veins, hosting muscovite and minor K-feldspar, albite and CGM, occurs in the Feli open pit to the north of the pegmatite field (Fig. 2b). Those veins are folded, discordant to the foliation of metasedimentary rocks and crosscut by undeformed Li-mica-rich spodumene-bearing pegmatite dykes (T9) (Roda-Robles *et al.,* 2010, 2023; Vieira *et al.,* 2011). Drilling in this location has revealed the presence of a hidden muscovite-bearing granitic body that was suggested as potential source for Feli cassiterite-rich veins (Roda-Robles *et al.*, 2009, 2023) (Fig. 3).

3 Methods

Detailed analytical protocols along with mineral compositions and U-Pb isotope data are provided in Supplementary files. Thick section chemical mapping was done by μ-XRF. Oxide mineral backscattered electron (BSE, for CGM and cassiterite) and cathodoluminescence (CL, for cassiterite) imaging were performed using a scanning electron microscope. Higher resolution chemical mapping of oxide minerals was performed by energy-dispersive X-ray spectroscopy (EDS) or wavelength-dispersive X-ray spectroscopy (WDS) using a scanning electron microscope and electron microprobe, respectively. Major and minor elemental abundances were determined by electron microprobe for CGM, cassiterite, micas and phosphates, and trace element abundances were measured by laser ablation-inductively coupled plasma mass spectrometry (LA-ICP-MS) for cassiterite. Cassiterite U-Pb geochronology was done by LA-ICP-MS using Yankee cassiterite as primary reference material (Carr *et al.*, 2020), and Jian-1 cassiterite as control material (Tapster and Bright, 2020), following the method of Carr *et al.* (2023). Columbite-group mineral U-Pb dating was performed by LA-ICP-MS using zircon crystals as reference (GJ1, Jackson *et al.,* 2004) and control (Plešovice, Sláma *et al.,* 2008; M127, Nasdala *et al.,* 2016) materials following the method described in Melleton *et al.* (2022). At the time of the analysis, no internationally recognized reference material was available for CGM. However, Melcher *et al.* (2008) did not observe significant matrix-dependent U-Pb fractionation when employing zircon as a primary reference material during CGM dating by LA-ICP-MS. This method generally provides age results consistent with those obtained through conventional matrix-matched U-Pb dating of other minerals such as monazite or apatite (Fosso Tchunte *et al.,* 2018; Marcoux *et al.,* 2021). Moreover, further investigations have revealed that matrix effects are primarily associated with tantalite compositions (Legros *et al.,* 2019), and CGM analyzed during this study mostly range in compositions from Fe- to Mn-columbite. U-Pb diagrams and ages were produced with IsoplotR (Vermeesch, 2018) with errors quoted at the 2-sigma level, ages including the estimated long-term reproducibility of 1.9% for cassiterite (Carr *et al.,* 2023).

4 Samples, textures, and F-mineral compositions

Samples were collected from Nb-Ta-Sn-oxide-mineral-bearing pegmatites over the FA area. Large quantities of cassiterite, along with CGM or rare pyrochlore-groupminerals,

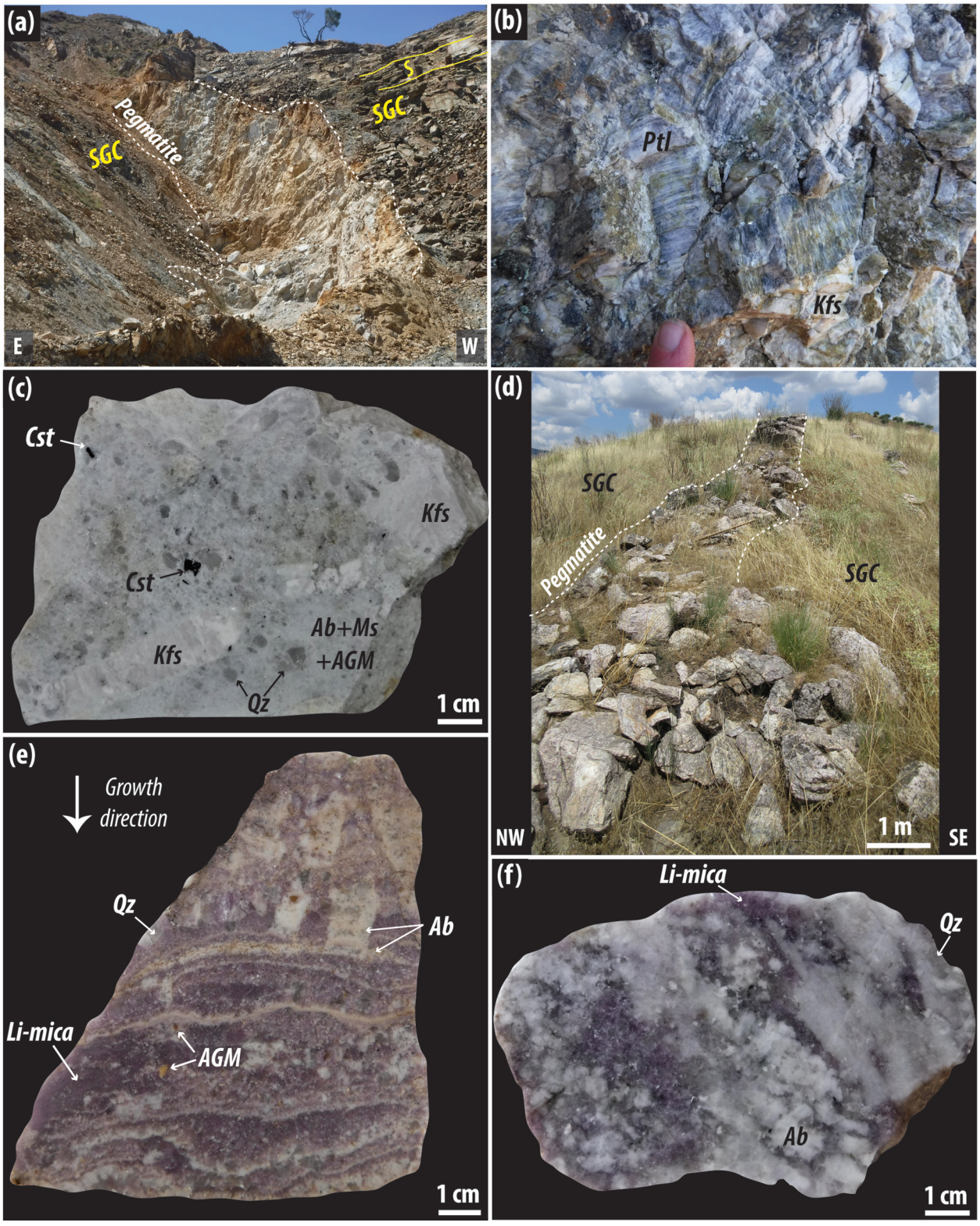

Fig. 4. Field and hand sample photographs of Li-mineralized pegmatites from the Fregeneda-Almendra pegmatite field. (a) Ten to 20 m thick petalite-rich pegmatite crosscutting the foliation (S) of micaschists from the Schist-graywacke Complex (SGC) at the Bajoca mine. (b) Petalite-rich pegmatite at the Hinojosa locality. (c) K-feldspar phenocrysts within a fine-grained assemblage of quartz-albite-amblygonite-group minerals (AGM) and cassiterite in petalite-rich pegmatite from the Bajoca mine. (d) Two-meter-thick Li-mica-rich pegmatite dyke intruding metasedimentary rocks from the SGS at the Ramalha-Est locality. (e) Layered Li-mica-rich AGM-bearing pegmatite (sample P010). The growth direction reflected by albite phenocrysts is indicated. (f) Li-mica-rich pegmatite from the Feli mine. Mineral abbreviation from Whitney and Evans (2010).

Table 1. Summary of pegmatite sample mineralogy, country-rock metamorphic zones and GPS coordinates (WGS84).

Locality	Sample	Metamorphic zone	Mineralogy	GPS coordinates	
				Y	X
Petalite-rich pegmatites					
Bajoca	-	Andalusite	Qz, Kfs, Ab, Ptl, Ms, Znw, AGM, Ap, Fe-Mn-Pho, Cra-Goy, Cst, CGM	41.0019	-7.01709
Plombal	P018	Andalusite	Qz, Kfs, Ab, Ptl, Ms, Ap, Cst, CGM	40.9969	-6.92849
Hinojosa	ALM-2	Biotite	Qz, Kfs, Ab, Ptl, Ms, Ap, Cst, CGM	41.0042	-6.81802
Ramalha	P016	Biotite	Qz, Kfs, Ab, Ptl, Ms, AGM, Ap, Fe-Mn-Pho, Cst, CGM	41.0023	-7.00754
Li-mica-rich pegmatites					
Ramalha-E	ALM-3	Biotite	Qz, Ab, Li-mica, Ms, KFs, AGM, Tpz, Cst, CGM	41.0027	-7.00684
-	P010	Biotite	Qz, Ab, Li-mica, (Spd), Ms, AGM, Ap, Cst, CGM	41.0152	-6.83753
Ramalha-W	P017	Biotite-chlorite transition	Qz, Kfs, Ab, Li-mica, Ms, Ap, Cst, PGM	41.0072	-7.01131
Feli	MF1001c	Chlorite	Qz, Ab, Li-mica, Spd, AGM, Cst, CGM	41.0276	-6.88704

Qz: quartz, Kfs: K-feldspar, Ab: albite, Ptl: petalite, Spd: spodumene, Ms: muscovite; Znw: zinnwaldite, Ap: apatite; AGM: amblygonite-group mineral, Ap: apatite, Fe-Mn-Pho: Fe-Mn-phosphate, Cra-Goy: crandallite-goyazite; Tpz: topaz, Cst: cassiterite, CGM: columbite-group mineral, PGM: pyrochlore-group mineral. Spodumene occurrences were described in the vicinity of P010 pegmatite dyke (Vieira et al., 2011) but this mineral was not observed in investigated sample.

were found in eight pegmatites, including four petalite-rich (T7 of Vieira *et al.*, 2011), two Li-mica-rich-spodumene-bearing (T9: Feli, P010) and two Li-mica-rich spodumene-free (T10: Ramala-West and −East) pegmatites (Figs. 2b and 4). For the remainder of this paper, we refer to the T9 and T10 pegmatites as Li-mica-rich pegmatites following the Iberian scale classification of Roda-Robles *et al.* (2018). Pegmatite sample mineralogy along with GPS coordinates are provided in Table 1 and a paragenetic sequence summarizing our textural observations and interpretations is provided in Figure 5.

Generally, Li-pegmatites do not display well-defined large-scale zoning, for example a wall zone or a quartz core that are common to other pegmatites deposits (London, 2014). However, petalite-rich pegmatites commonly have a heterogeneous texture with large (> 2 cm) subhedral to anhedral crystals of K-feldspar and petalite, occurring in a finer-grained (< 1 cm) matrix mostly consisting of albite, quartz, muscovite, phosphate and oxide minerals (Fig. 4b, c). K-feldspar phenocrysts show resorption textures and are partially replaced by albite (Fig. 6a, b), and AGM are corroded by muscovite (Fig. 7a). Moreover, F-apatite, along with rare Al-Sr-Ca-F phosphates (probably a solid solution between crandallite and goyazite ; Roda-Robles *et al.*, 2010), commonly occur as alteration products around AGM and Fe-Mn-phosphates (Figs. 6a, b and 7b). Moreover, as previously noted by Vieira *et al.* (2011), zinnwaldite (a Fe-F-Li-rich trioctahedral mica, Fig. 8) was found as small secondary overgrowths on muscovite in the Bajoca petalite-rich pegmatite (Fig. 7a, b).

Li-mica-rich pegmatites (or aplo-pegmatites) commonly show unidirectional solidification textures forming a layering marked by the alternation of Li-mica-rich and quartz-albite-rich millimeter to centimeter thick zones parallel to the contact with the country-rock (Figs. 4e and 6c). K-feldspar was found as anhedral crystal relics, partly replaced by albite, Li-mica and quartz, within the Ramalha-W pegmatite, and as inclusions within topaz in the Ramalha-E pegmatite (Fig. 7c). Most topaz and AGM appear to have crystallized relatively early as they are partially resorbed by Li-micas (Fig. 7c, d).

Amblygonite-group minerals in both pegmatite types do not contain detectable Na and overlap in F concentrations between 0.25 and 0.45 atoms per formula unit (apfu) (Supplementary File 2). However, AGM from P010 and Ramalha-E Li-mica-rich pegmatites reach slightly higher F concentrations than that from the petalite-rich Bajoca pegmatite (< 0.4 apfu). Some AGM crystals in the P010 pegmatite have low F contents < 0.3 apfu and possibly experienced subsolidus alteration (*e.g.*, London and Burt, 1982).

Dioctahedral mica flakes in petalite-rich pegmatites have a typical muscovite composition, Ti contents up to 0.02 apfu (based on 22 oxygen atoms) and relatively low F concentrations below 0.3 apfu (Fig. 8). Conversely, micas in Li-mica-rich pegmatites are mostly trioctahedral Li-muscovite to lepidolite (classification of Tischendorf *et al.*, 1997, not shown) with 1 to 3 apfu F, and Ti contents < 0.01 apfu. Those micas are locally patchy zoned with dioctahedral micas (muscovite) having relatively low F of ~0.1–1 apfu. Micas in Li-mica-rich pegmatites are enriched in Mn relative to Fe (Mn *minus* Fe ≥ 0 apfu) compared to that from petalite-rich pegmatites (Mn − Fe < 0 apfu) (Fig. 8).

5 Oxide mineral textures

Cassiterite and CGM were observed together in most samples, except in Plombal petalite-rich and Ramalha-W Li-mica-rich pegmatites where CGM are rare or absent (Tab. 1; Figs. 6, 9 and 10). Pyrochlore-group minerals with a fluorcalciomicrolite composition were found in the Ramalha-W pegmatite (Fig. 9e). In the studied samples, oxide minerals are generally coarser in petalite-rich pegmatites than in Li-mica-rich pegmatites. Cassiterite commonly forms large, 0.5 to 5 mm in size, subhedral to anhedral short prismatic crystals whereas CGM generally occur as numerous small, tens

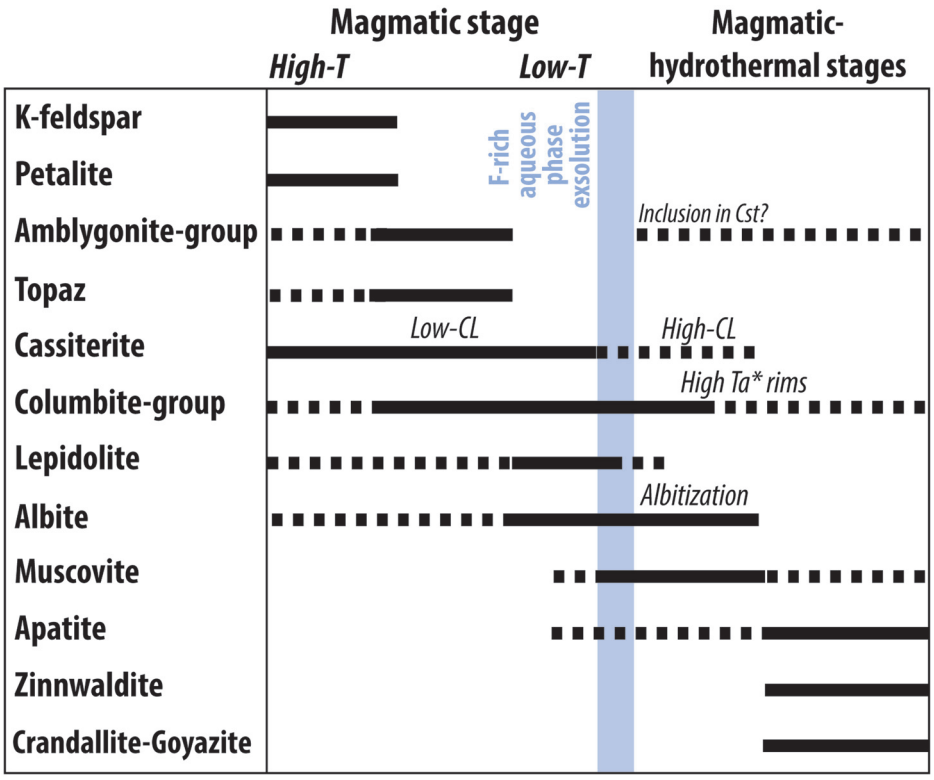

Fig. 5. Paragenetic sequence summarizing textural observations and interpretations for investigated samples of petalite-rich and Li-mica-rich pegmatites from the FA pegmatite field. See also the paragenetic sequence of Errandonea-Martin *et al.* (2022) for more detailed interpretations regarding the magmatic-hydrothermal evolution of FA pegmatites.

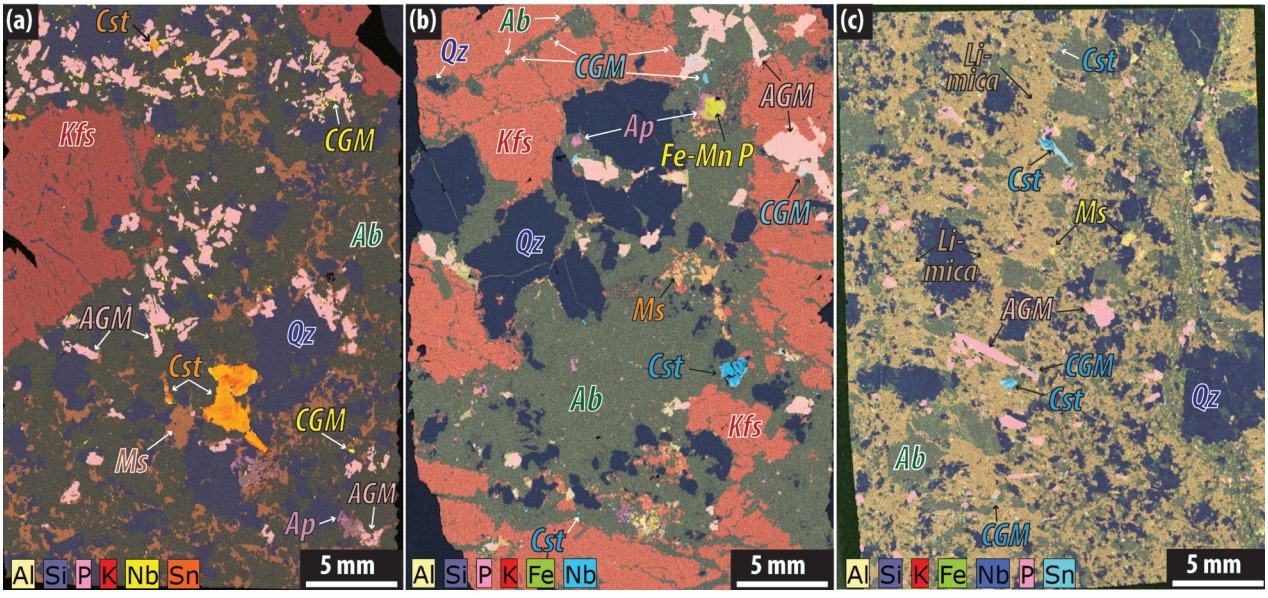

Fig. 6. Composite chemical maps of thick sections of (a) Bajoca petalite-rich pegmatite, (b) Ramalha petalite-rich pegmatite (P016) and (c) Li-mica-rich pegmatite (P010). Note the partial replacement of K-feldspar and cassiterite phenocrysts by albite (a,b) as well as albite-quartz-columbite-group mineral (CGM) vein crosscutting K-feldspar (b). CGM tend to be spatially associated to amblygonite-group minerals in (a-b) and apatite occurs as alteration product around AGM (a) and Fe-Mn phosphates (b).

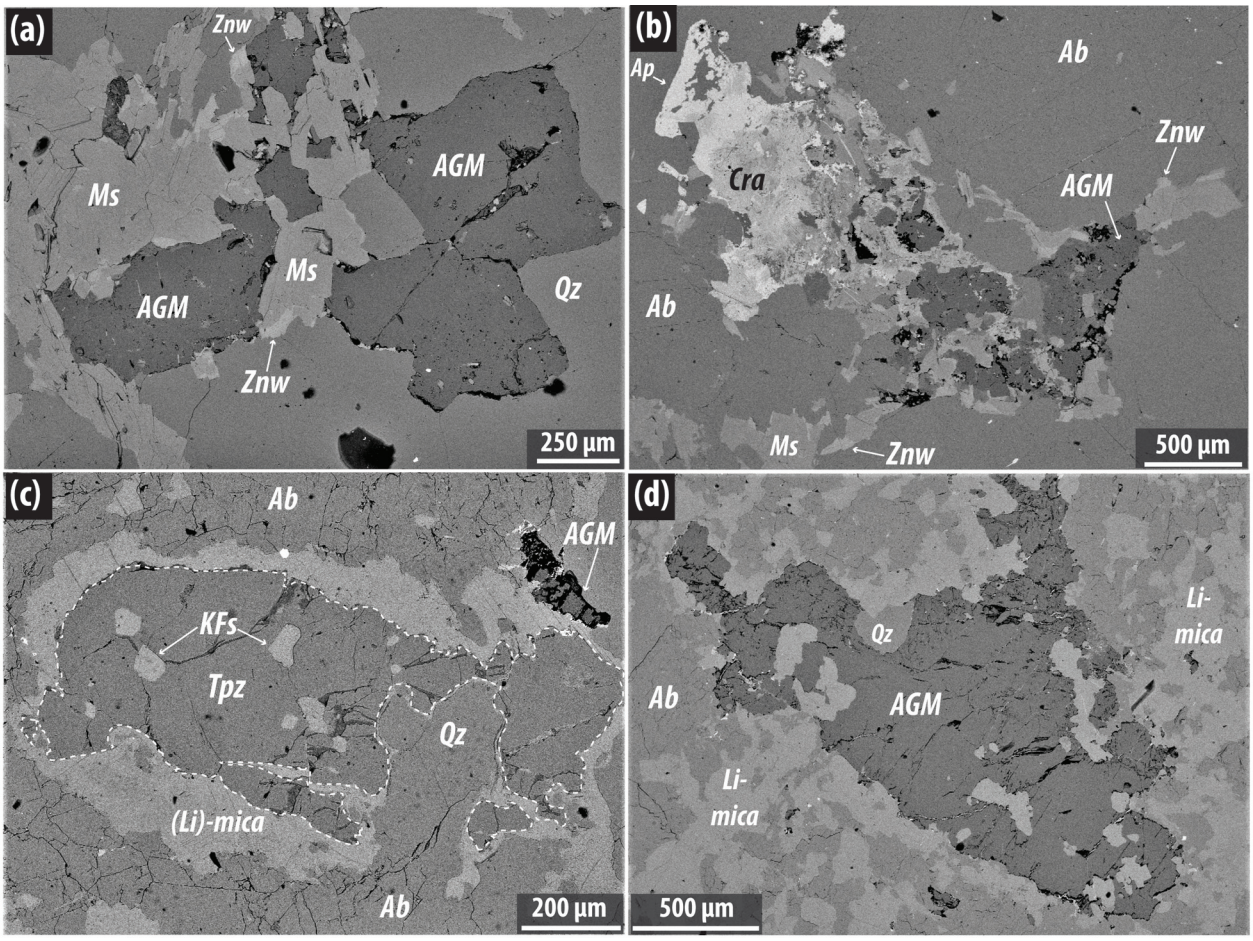

Fig. 7. Backscattered electron images showing textural occurrences of F-rich minerals in FA Li-pegmatites. (a-b) Bajoca petalite-rich pegmatite: amblygonite-group minerals (AGM) partially resorbed by muscovite, and secondary zinnwaldite overgrowths on muscovite; (b) Secondary F-apatite and Al-F-Sr-Ca phosphates (likely crandallite-goyazite: Cra) surrounding AGM. (c-d) Ramalha-E Li-mica-rich pegmatite (ALM-3): (c) topaz (Tpz), hosting K-feldspar inclusions, corroded by quartz and micas with muscovite to lepidolite compositions; (d) AGM partially replaced by Li-micas.

of micrometers to 1 mm in size, elongated prismatic crystals. Cassiterite crystals are commonly partially resorbed by albite and micas (Figs. 6a). Columbite-group minerals tend to cluster with AGM, especially in petalite-rich pegmatites, suggesting that most CGM crystallized along with or slightly after AGM (Figs. 6 and 9a). However, some CGM probably crystallized later as reflected by the local occurrence of albite-quartz-CGM-bearing veins crosscutting K-feldspar (Fig. 6b).

Columbite-group minerals are characterized by variably complex internal textures and are commonly overgrown with rim structures or show intra-crystal mantles with bright BSE signals that are enriched in Ta relative to Nb (Fig. 9). In CL images, cassiterite crystals from petalite- and Li-mica-rich pegmatites commonly show a core characterized by dark color and growth zonation (Fig. 10). This low-CL cassiterite core is locally brecciated and overgrown by cassiterite with yellow CL color that may have patchy or oscillatory zoning. The high-CL cassiterite hosts inclusions of concentrically zoned CGM, albite, mica, quartz and rare AGM, whereas the low-Cl cassiterite is inclusion-free. The high-CL cassiterite is depleted in Nb, Ta, Mn and Fe compared to the low-CL cassiterite (Fig. 10).

6 Oxide mineral compositions

Columbite-group minerals from petalite-rich pegmatites are mostly columbite-Fe, with $Mn/(Mn+Fe)_{apfu}$ ratios, or Mn*, between ~0.05 and 0.60, whereas the large majority of CGM from Li-mica-rich pegmatites are columbite-Mn with Mn* values close to 1 (Fig. 11a). The range of $Ta/(Nb+Ta)_{apfu}$ ratios, or Ta*, of CGM within each pegmatite sample is comparable and vary from ~0.05 to 0.6, with the highest Ta* values generally occurring in CGM rims or mantles. Columbite-group mineral inclusions within high-CL cassiterite from the Bajoca petalite-rich pegmatite have slightly lower Mn* values (0.03–0.13) than discrete CGM crystals from the same pegmatite (~0.1–0.50). However, such compositional difference is not observed between CGM inclusions in cassiterite and discrete CGM from Li-mica-rich pegmatites. Columbite-group minerals from the different petalite-rich pegmatites show distinct geochemical signatures. Their mean Mn* and Ta* values increase from the Bajoca pegmatite emplaced in the andalusite zone ($Mn_{mean}^* = 0.21$, $Ta_{mean}^* = 0.14$) to the Hinojosa (0.33, 0.20) and Ramalha

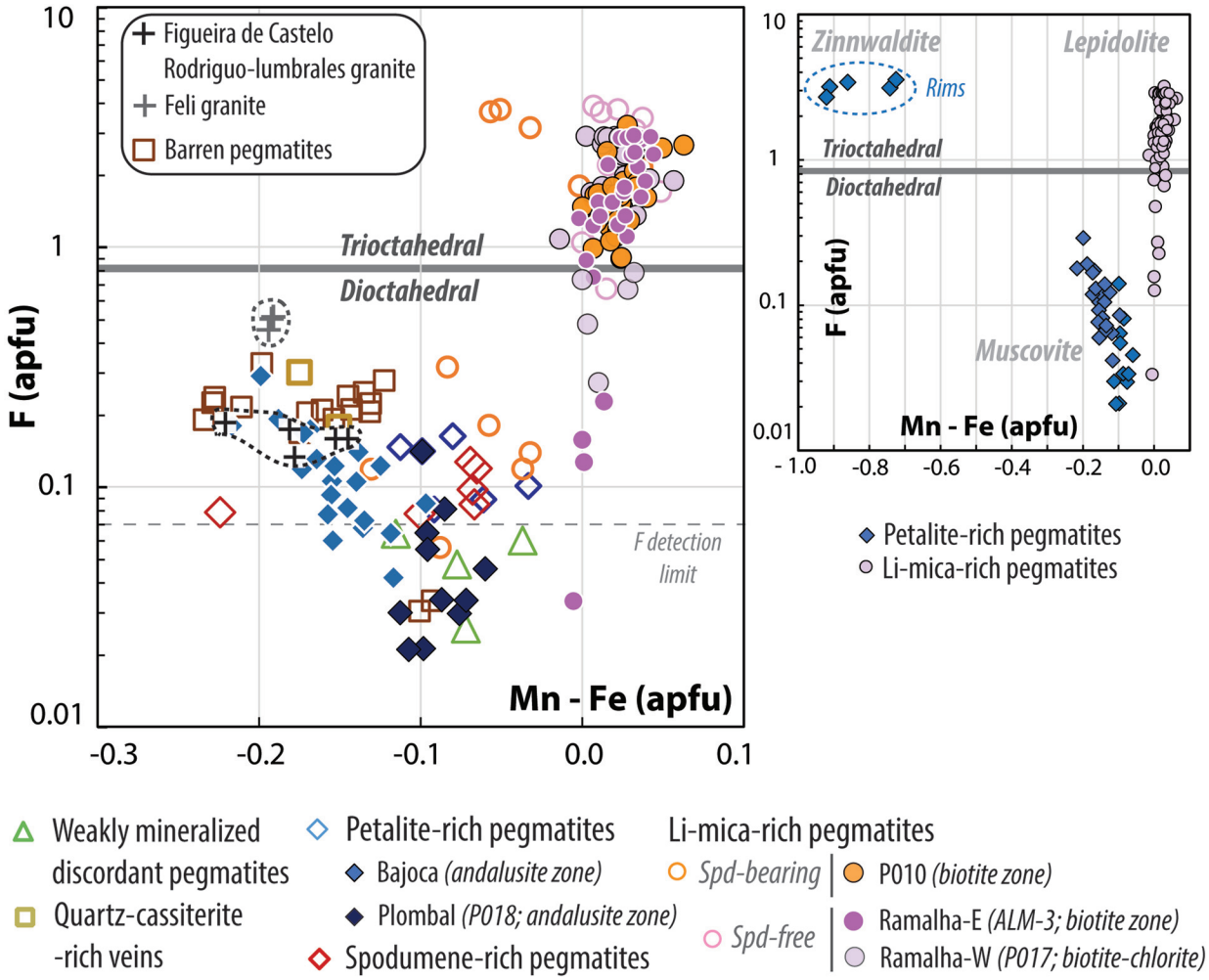

Fig. 8. Compositions of micas from pegmatites of the FA pegmatite field, as well as spatially associated leucogranites, in F vs Mn − Fe diagrams (apfu). Filled symbols represent data from this study, and empty symbols and crosses (granites) are from Vieira (2010).

(0.45, 0.33) pegmatites emplaced within the biotite zone (Fig. 2b). In Figure 11b, the Sn concentrations of CGM broadly correlate with their Ti contents for petalite-rich pegmatites, and CGM from the Bajoca pegmatite reach higher Ti concentrations than that from other pegmatites of the same type. Columbite-group minerals from Li-mica-rich pegmatites are characterized by lower Ti contents than CGM from petalite-rich pegmatites, but have a similar range of Sn concentrations that do not correlate with their Ti contents. Few CGM were analyzed for their Zr concentrations; CGM from the Feli Li-mica-rich pegmatite contain minor amount of Zr up to 0.03 apfu (0.7 wt%) whereas Zr is below 0.01 apfu (0.07 wt%) in Bajoca petalite-rich pegmatite CGM (Supplementary File 2).

Cassiterite from both pegmatite types reaches relatively high Nb + Ta concentrations up to 0.1 apfu (~7 wt%) that correlate with Mn + Fe contents (Fig. 12a). However, cassiterite from both pegmatite types defines distinct geochemical trends, whereby compositions from Li-mica-rich pegmatites tend to plot above the CGM substitution line and are relatively enriched in Nb + Ta at given Mn + Fe contents compared to that from petalite-rich pegmatites (Fig. 12a). Cassiterite from Li-mica-rich pegmatites are characterized by significantly higher Mn/Fe (0.1–90) ratios, Zr (300–2500 ppm) and Ga concentrations (> ~10 ppm) along with lower Ti/Zr ratios (< ~0.6) and Ti concentrations (30–640 ppm) than cassiterite from petalite-rich pegmatites (Mn/Fe < ~0.1; Ti/Zr > ~0.6; Zr ~130–1000 ppm; Ga < ~10 ppm; Ti ~200–3400 ppm; Figs. 12c and 13). However, cassiterite from both pegmatite types shows similar Nb/Ta ratios (0.3–9.0) as well as Nb and Ta concentrations (Fig. 13). At the pegmatite field scale, cassiterite roughly evolves toward lower Ti concentrations and Ti/Zr ratios, and higher Mn/Fe ratios from petalite-rich pegmatites emplaced in the andalusite zone (Bajoca-Plombal) to that emplaced in the biotite zone (Hinojosa-Ramalha) (Figs. 12c and 13). Regarding Li-mica-rich pegmatites, cassiterite from the Feli pegmatite, emplaced in the chlorite zone, is characterized by higher Mn/Fe ratios than that from P010 (biotite zone) and Ramalha-W (biotite-chlorite zone transition) pegmatites. In the Bajoca pegmatite, early, low-CL, cassiterite shows significantly higher Nb/Ta ratios as well as Ga, Nb, Ta, Mn and Fe concentrations than late, high-CL, cassiterite, whereas differences in terms of Mn/Fe ratios and Ti concentrations are only minor between both cassiterite generations (Figs. 12b,c and 13).

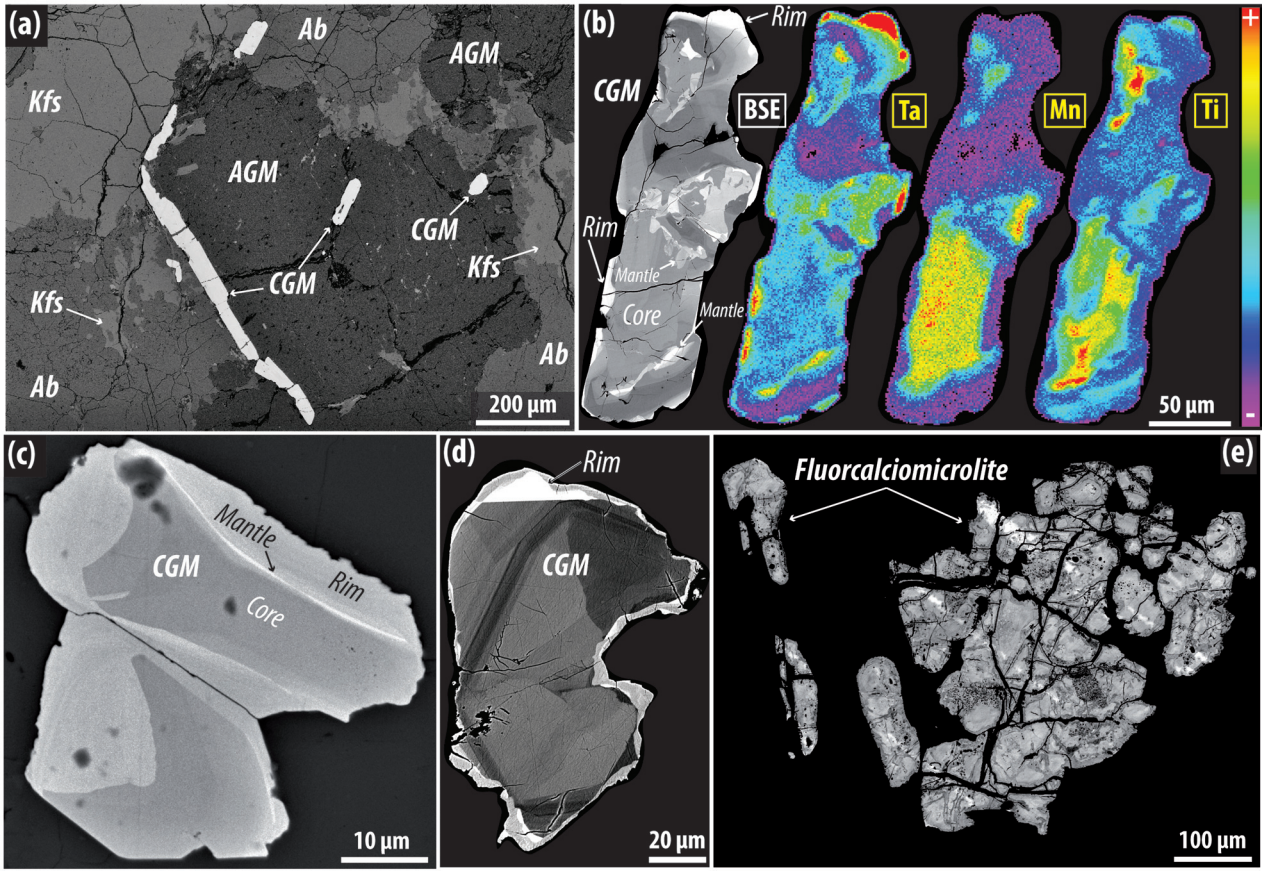

Fig. 9. Backscattered electron images and chemical maps (b) of Nb-Ta oxide minerals from FA Li-pegmatites. (a) Columbite-group minerals (CGM) in association with albite and amblygonite-group minerals (AGM) in the Ramalha petalite-rich pegmatite (P016). Note relics of K-feldspar in albite. (b-d) Variably zoned CGM crystals from (b-c) the Bajoca petalite-rich pegmatite and (d) P010 Li-mica-rich pegmatite. Note rims or mantles with light BSE signals reflecting high Ta/Nb ratios. (e) Fluorcalciomicrolite from the Ramalha-West (P017) Li-mica-rich pegmatite.

7 Cassiterite and columbite-group mineral U-Pb geochronology

Cassiterite is variably enriched in common Pb and plots in concordant to highly discordant position in Tera-Wasserburg diagrams (Fig. 14). In all samples, cassiterite analyses define discordia lines allowing to calculate lower intercept ages mostly ranging from 315 ± 6 Ma to 308 ± 6 Ma (Tab. 2). In Bajoca and Hinojosa petalite-rich pegmatites as well as in Li-mica-rich pegmatites, some discordant analyses plot outside of the discordia lines defined by most analyses. Those data, interpreted to reflect secondary disturbances of the U-Pb isotopic composition such as the loss of U or Pb (Fig. 14a), were excluded from lower intercept age calculations. Two samples, including Ramalha-W and Ramalha-E Li-mica-rich pegmatites, provide intercept ages of 312 ± 7 Ma and 310 ± 25 Ma with high MSWD values of 6.8 and 4.6, respectively, reflecting individual geological age dispersion (Fig. 14). However, those intercept ages are comparable to intercept ages yielded by other samples, supporting their geological significance.

The discordia lines defined by cassiterite analyses mostly return initial $^{207}Pb/^{206}Pb_{(0)}$ compositions between 0.83 ± 0.02 and 0.87 ± 0.01 globally in agreement with the model terrestrial Pb isotope composition at 310 Ma (*i.e.*, $^{207}Pb/^{206}Pb_{(310)}$ ~0.86; Stacey and Kramers, 1975) (Fig. 14 and Tab. 2). However, cassiterite from the Plombal pegmatite yields a weakly constrained and abnormally high $^{207}Pb/^{206}Pb_{(0)}$ ratio of 1.09 ± 0.7, due to the sub-concordant to concordant character of most of the analyses (Fig. 14c). Therefore, although identical within error, we recommend the use of the concordia age of 315 ± 6 Ma over the lower intercept age of 314 ± 6 Ma for the Plombal pegmatite. In the Bajoca pegmatite, cassiterite yields also similar concordia and lower intercept ages of 317 ± 6 and 315 ± 6 Ma, respectively (Fig. 14a). We nevertheless recommend the use of the lower intercept age over concordia age for data interpretation in this case as it takes into account a higher number of analyses and yield a geologically reasonable $^{207}Pb/^{206}Pb_{(0)}$ of 0.87 ± 0.01. Analyses performed on high-CL cassiterite from the Bajoca pegmatite are strongly discordant partly due to low U concentrations generally < 1 ppm, and provide a poorly

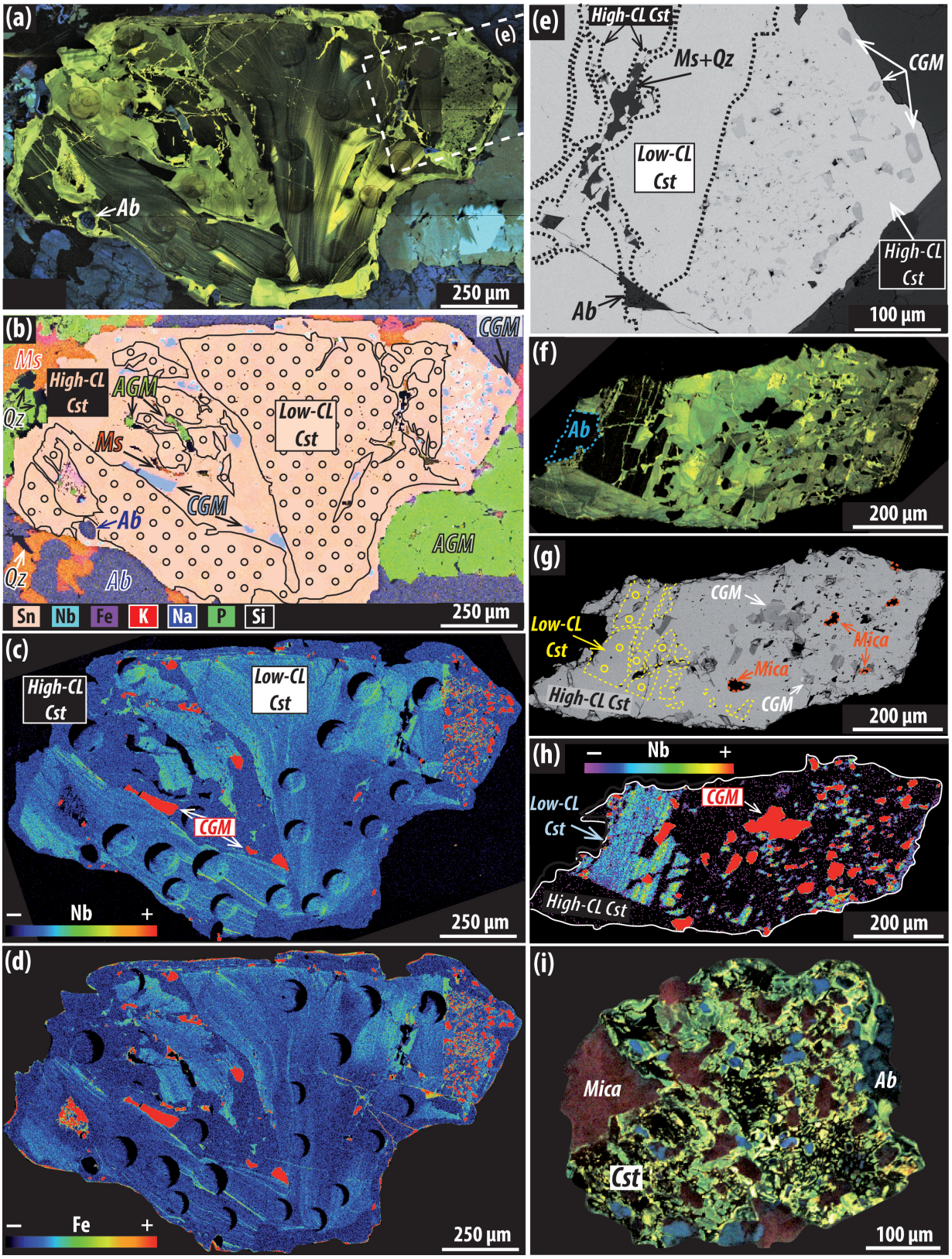

Fig. 10. Cathodoluminescence (a, f, i) and BSE images (e, g), as well as EDS (b) and WDS (c-d, h) chemical maps of cassiterite from FA Li-pegmatites. (a-e) Cassiterite crystal from the petalite-rich Bajoca pegmatite showing a Nb-Fe-rich core with low CL signal brecciated by high-CL, Nb-Fe-poor, cassiterite. The low-CL cassiterite is inclusion-free whereas the high-CL cassiterite hosts inclusions of columbite-group minerals (CGM), muscovite, albite, quartz and amblygonite-group minerals (AGM). (f-h) Low-CL, Nb-Mn-rich, cassiterite brecciated by high-CL, Nb-Mn-poor, cassiterite hosting CGM, mica and albite inclusions from the Li-mica-rich Feli pegmatite. (i) Cassiterite breccia from the Feli pegmatite consisting of low- and high-CL cassiterite (black to yellow), albite (blue) and mica (red).

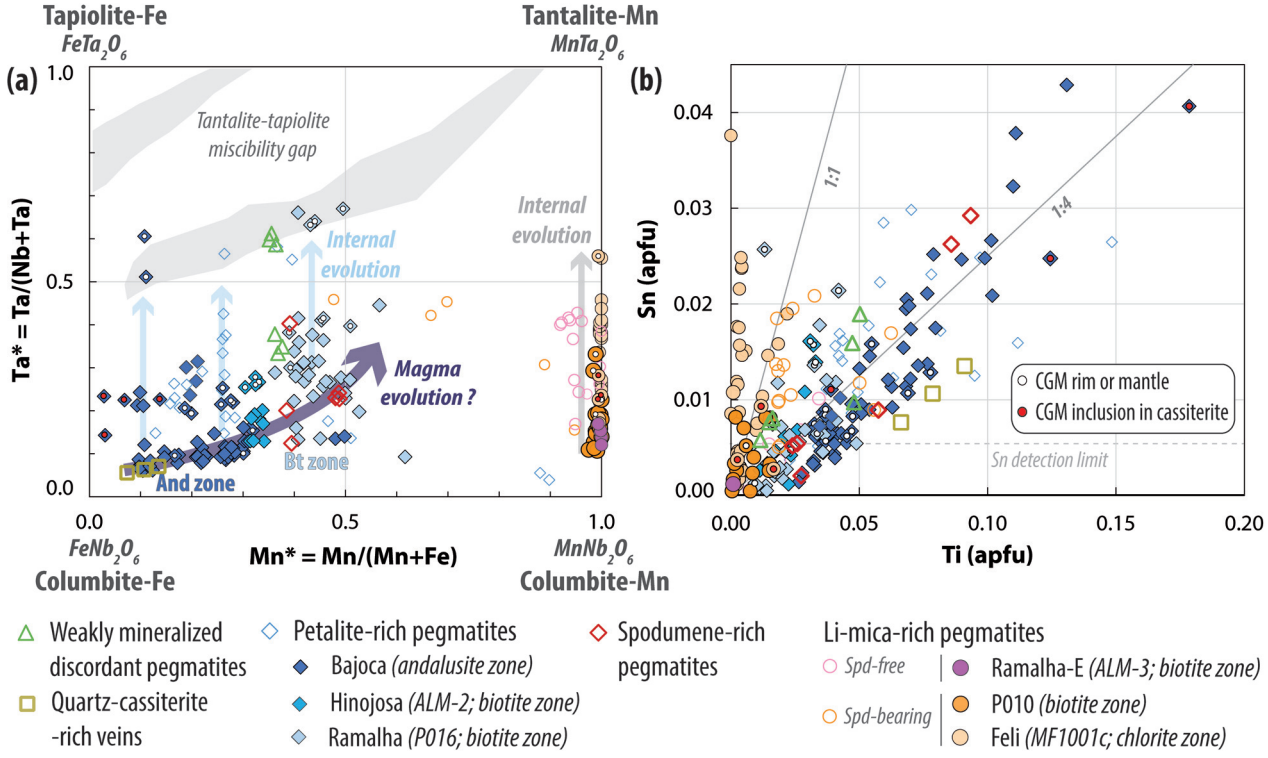

Fig. 11. Chemical composition of columbite-group minerals from pegmatites of the FA field. Filled and empty symbols represent data from this study and the literature (Roda-Robles *et al.*, 1999; Vieira 2010), respectively. (a) Ta/(Nb+Ta) *versus* Mn/(Mn+Fe) diagram (apfu) with tantalite-tapiolite miscibility gap from Van Lichtervelde *et al.* (2018). Evolution trends of CGM compositions interpreted as reflecting, either magma differentiation at the scale of the pegmatite field, or internal evolution after pegmatite-forming magma emplacement, including late-magmatic to magmatic-hydrothermal processes, are indicated. CGM crystal rims or mantles as well as CGM in inclusions in cassiterite (see Figs. 9 and 10) are distinguished with a white and red dot, respectively. (b) Sn *versus* Ti diagram (apfu).

constrained lower intercept age of 300 ± 27 Ma (MSWD = 22) (Fig. 14a, Supplementary material 4). In contrast, low-CL cassiterite (U ~ 5–25 ppm) yields a lower intercept age of 315 ± 6 Ma (MSWD = 0.3) identical to that calculated by combining both cassiterite generations from this pegmatite.

Discrete CGM crystals of ~100–500 µm in size were handpicked from the petalite-rich Bajoca pegmatite (MB1001b) and Li-mica-rich Feli pegmatite (MF1001C). No differences in terms of U-Pb isotope composition can be attributed to CGM zoning. Columbite-group mineral analyses from the Bajoca pegmatite plot in sub-concordant to slightly discordant position in the Tera-Wasserburg diagram and yield a mean $^{206}Pb/^{238}U$ age of 309 ± 3 Ma (n=8, MSWD = 0.5; Fig. 15a). Analyses of CGM from the Feli pegmatite are concordant to sub-concordant. The seven most concordant analyses (discordance ≤ 3%) yield a concordia age of 308 ± 5 Ma (MSWD = 1.0) identical to the lower intercept age of 308 ± 4 Ma (MSWD = 1.2) and mean $^{206}Pb/^{238}U$ age of 308 ± 3 Ma (MSWD = 0.4) calculated using all analyses (n = 15, Fig. 15b). Columbite-group mineral U-Pb ages are identical within error to the cassiterite lower intercept U-Pb ages obtained on the Bajoca (315 ± 6 Ma) and Feli (310 ± 6 Ma) pegmatites (Fig. 14).

8 Discussion

8.1 Oxide mineral crystallization

Cassiterite crystals from Li-pegmatites of the FA field are locally partially resorbed by albite (Fig. 6a), and commonly show evidence for metasomatic overprint with low-CL cores brecciated by high-CL cassiterite relatively depleted in Nb, Ta, Fe and Mn (Figs. 10 and 12). The low-CL cassiterite cores, that are inclusion-free, are interpreted to have crystallized at the magmatic stage, along with or slightly after K-feldspar phenocrysts (Fig. 5). Cassiterite with likely magmatic origin has been documented in several peraluminous rare-metal granites and pegmatites (Cuney *et al.*, 1992; Linnen and Cuney, 2005). Its crystallization, reflecting a decrease of Sn solubility, has been interpreted to reflect the low solidus temperature of the flux-rich parental melts of those intrusions along with an increase of oxygen fugacity (Linnen *et al.*, 1996; Bhalla *et al.*, 2005; Pichavant, 2022). In contrast, the late, high-CL, cassiterite of the FA pegmatites notably hosts inclusions of albite, muscovite, CGM and quartz (Fig. 10). This suggests that the high-CL cassiterite formed in relationship with the albitization process that affected K-feldspar, and this

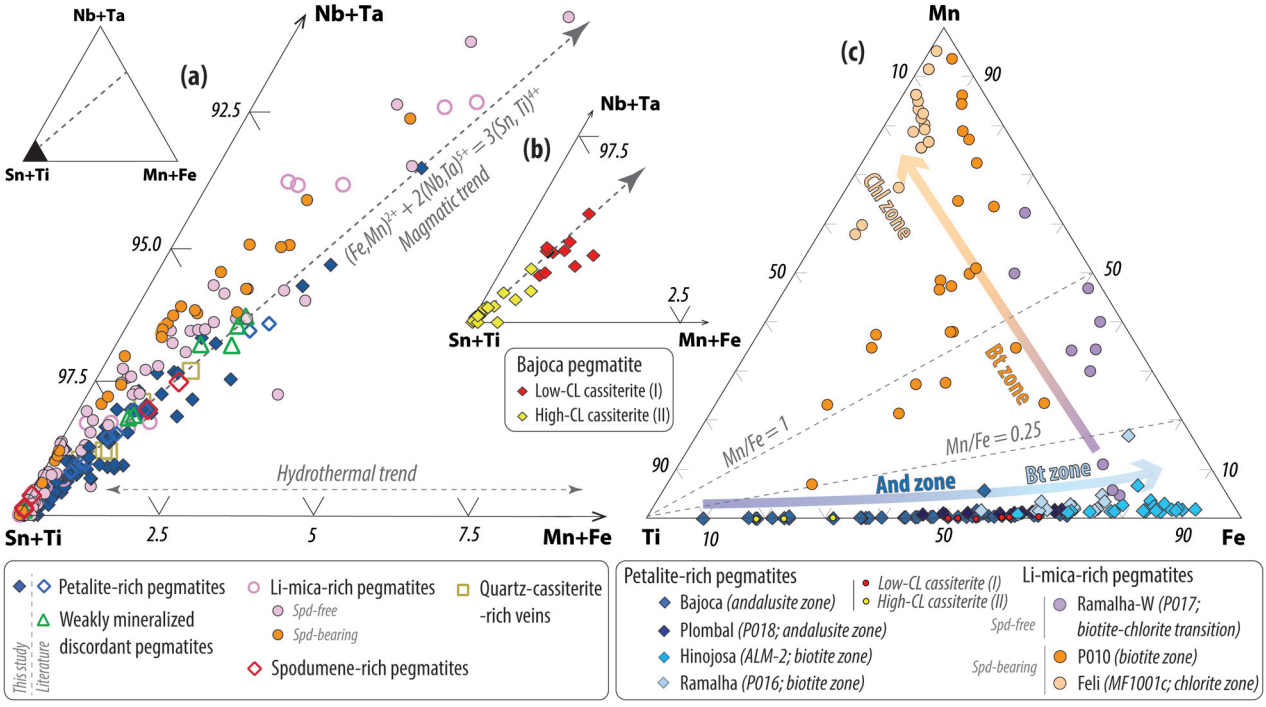

Fig. 12. Ternary diagrams showing the compositions of cassiterite from pegmatites of the FA field. (a-b) Nb + Ta *versus* Sn + Ti *versus* Mn + Fe diagram (apfu) comparing (a) the compositions of cassiterite from different pegmatite types, and (b) the compositions of early, low-CL, cassiterite with late, high-CL, cassiterite from the Bajoca petalite-rich pegmatite. Compositions are based on electron microprobe analyses from this study (filled symbols) and the literature (empty symbols; Roda-Robles *et al.*, 1999; Vieira 2010). The substitution line $(Fe,Mn)^{2+} + 2(Nb, Ta)^{5+} = 3(Sn,Ti)^{4+}$ is from Černý and Ercit (1985), and the magmatic and hydrothermal trends are from Marcoux *et al.*, (2021). (c) Fe *versus* Ti *versus* Mn diagram (ppm) comparing the compositions of cassiterite from different pegmatites, based on LA-ICP-MS analyses. Cassiterite compositional trends for petalite- and Li-mica-rich pegmatites in possible relation with the vertical distance of migration of their parent magma are shown as arrows.

metasomatism was also accompanied by the crystallization of micas and quartz (Figs. 6a-b). The Nb-Ta-Fe-Mn component of CGM inclusions/exsolutions in high-CL cassiterite likely originates, at least partly, from the destabilization of early, low-CL, cassiterite cores that are relatively enriched in Nb-Ta and Fe or Mn (Fig. 10). However, a significant part of those elements might have been brought by the albitizing fluid (or hydrosaline melt), as suggested by the local occurrences of albite-quartz-CGM-bearing veins crosscutting K-feldspar in petalite-rich pegmatites (Fig. 6b).

In contrast to low-CL cassiterite, a well constrained U-Pb age cannot be obtained from high-CL cassiterite alone, partly due to its relatively low U, and thus, low radiogenic Pb concentrations (Fig. 14a). Despite the absence of absolute age constrains, albitization is a well-documented magmatic-hydrothermal phenomena of rare-metal pegmatite systems worldwide including the FA pegmatites (Errandonea-Martin *et al.*, 2022). Such auto-metasomatism is commonly thought to occur during or at the end of pegmatite-forming magma crystallization due to the exsolution of a Na-rich hydrosaline melt or fluid (Dewaele *et al.*, 2011; Kaeter *et al.*, 2018; Müller *et al.*, 2018; Ballouard *et al.*, 2020a; Errandonea-Martin *et al.*, 2022). Therefore, the age difference between magmatic, low-CL, and magmatic-hydrothermal, high-CL, cassiterite might be indistinguishable considering the precision of LA-ICP-MS dating technique and the duration for the crystallization of pegmatite bodies generally expected to be lower than 1 Ma (*e.g.*, London, 2018).

Like cassiterite, discrete CGM crystals from FA Li-pegmatites commonly show complex zoning with small overgrowths or intra-crystal mantles with relatively high Ta* values, representing mostly dissolution-reprecipitation textures (Figs. 9 and 11). Such features may be the effect of disequilibrium crystallization (Van Lichtervelde *et al.*, 2018) or the interaction with an aqueous media, including a hydrosaline melt or late-magmatic fluid phase (Kaeter *et al.*, 2018; Ballouard *et al.*, 2020a). Therefore, CGM likely crystallized both at the magmatic stage (*i.e.*, discrete CGM cores) and magmatic-hydrothermal stage (*i.e.*, discrete CGM rims and CGM in inclusion in cassiterite or in veins) (Fig. 5). U-Pb dating of zoned and unzoned discrete CGM crystals yield consistent U-Pb ages with low MSWD values (≤ 1.0, Fig. 15) suggesting that the time differences between these two stages cannot be resolved with the current method precision.

8.2 Timing and tectonic-magmatic context of pegmatite-forming magmatism

Cassiterite and CGM U-Pb geochronology of both petalite-rich and Li-mica-rich pegmatites from the FA field yields ages from 315 ± 6 Ma (Bajoca and Plombal petalite-rich pegmatite cassiterite) to 308 ± 6 Ma (Hinojosa

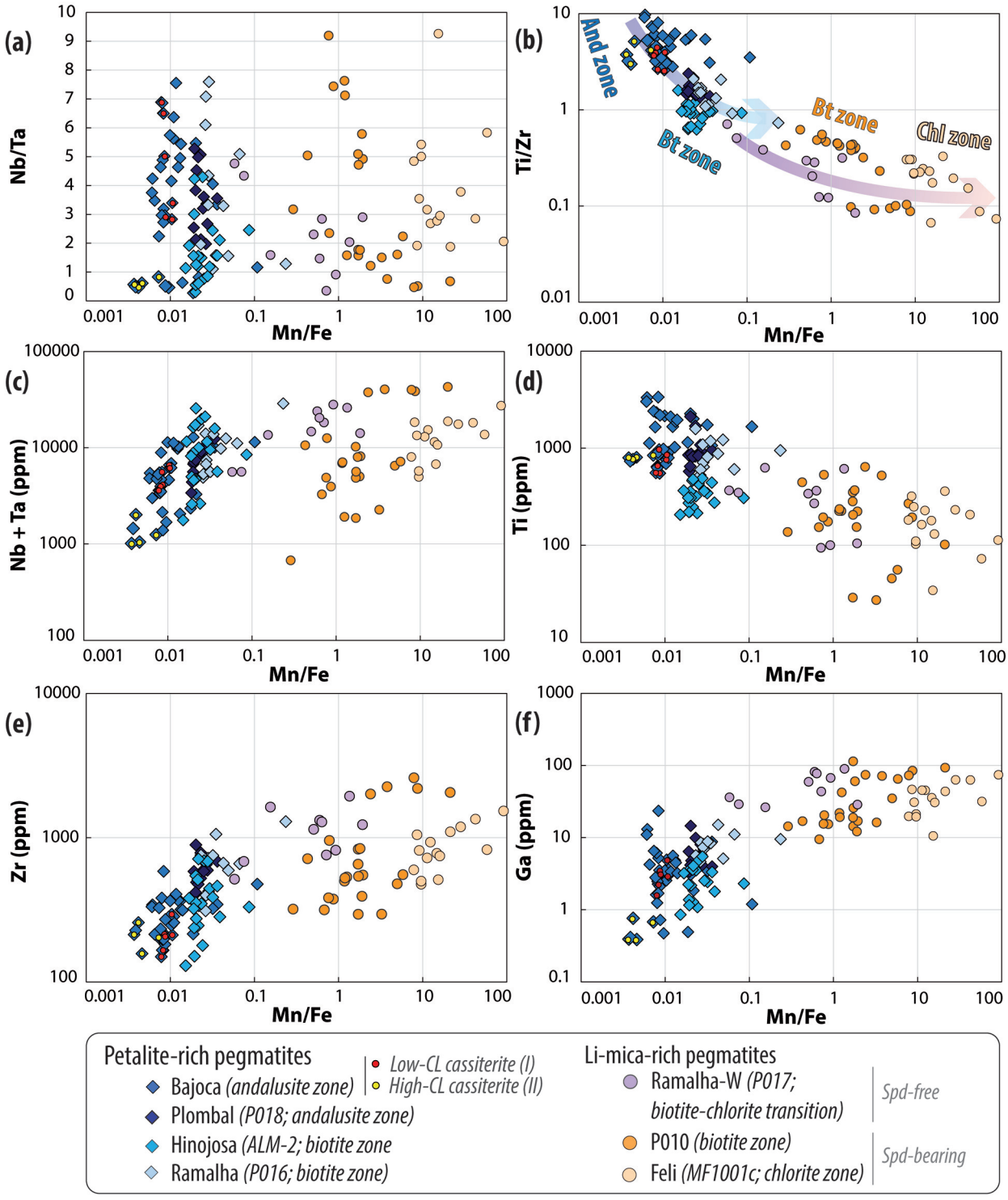

Fig. 13. Evolution of the Fe/Mn ratios of cassiterite from pegmatites of the FA field in function of selected trace element ratios and concentrations (based on ppm contents from LA-ICP-MS analyses). Composition trends for petalite- and Li-mica-rich pegmatites in possible relation with the vertical distance of migration of their parent magma are shown as arrows in (b). Compositions of early, low-CL, and late, high-CL, cassiterite from the Bajoca pegmatite are distinguished.

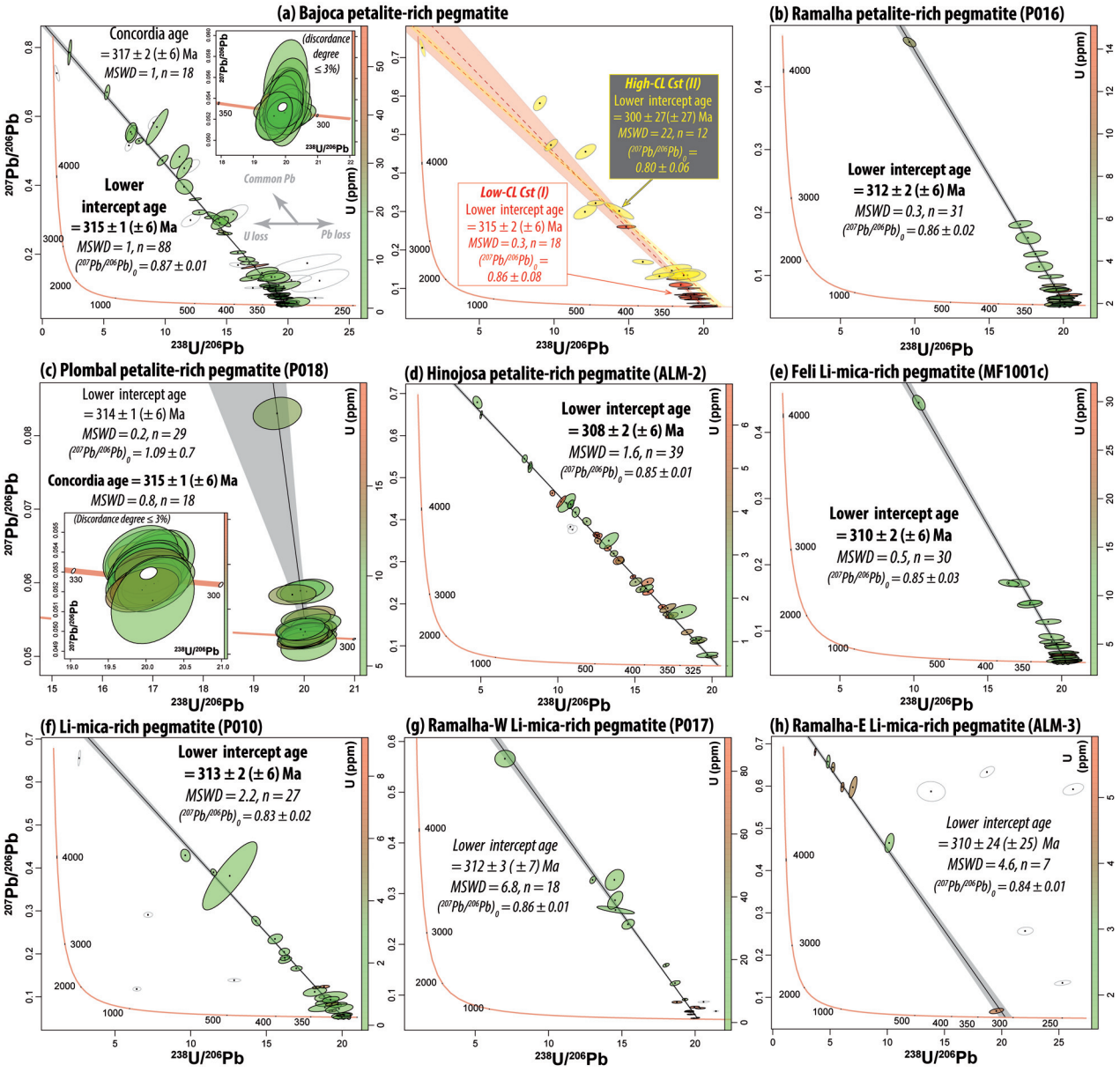

Fig. 14. Tera-Wasserburg diagrams showing the U-Pb compositions of cassiterite from pegmatites of the Fregeneda-Almendra field. The compositions of early, low-CL, and late, high-CL, cassiterite are distinguished for the Bajoca pegmatite (a). Ellipse and ages are reported at 2σ, with error between brackets including the long-term variance of cassiterite validation material (see Supplementary file for details). Ellipse color represents semi-quantitative U concentrations. Colorless ellipses interpreted as reflecting Pb or U losses were not used for age calculations. The concordia ages of the Plombal and Bajoca pegmatites were calculated considering cassiterite analyses with a degree of discordance $\leq$ 3%.

petalite-rich pegmatite cassiterite) that are identical within uncertainty (Fig. 16 and Tab. 2). Those ages are slightly older but overlap within uncertainty with the CGM U-Pb age of 302 ± 3 Ma obtained by Roda-Robles *et al.* (2023) on one crystal from the Carmen Li-mica-rich pegmatite from the FA pegmatite field (Fig. 16). The cassiterite and CGM U-Pb systems yield an older age range than the previously applied muscovite or Li-mica $^{40}Ar/^{39}Ar$ geochronometer with ages from 305 ± 4 to 295 ± 4 Ma for the pegmatite field, and ages between 297 ± 4 and 295 ± 4 Ma for petalite- and Li-mica-rich pegmatites (Roda-Robles *et al.*, 2009, 2023; Vieira, 2010) (Fig. 16). Pegmatite cassiterite and CGM U-Pb ages overlap with zircon U-Pb ages of the main two-mica-bearing leucogranite facies from the FCL anatectic complex emplaced from 317 ± 2 to 313 ± 2 Ma (Ferreira *et al.*, 2019), and with the youngest ages of zircon crystallization in FCL migmatites (344 ± 3 to 315 ± 1 Ma; Ferreira *et al.*, 2022) (Fig. 16). The mica $^{40}Ar/^{39}Ar$ age range of FA pegmatites is comparable to: (i) the muscovite $^{40}Ar/^{39}Ar$ age of 311 ± 4 Ma of a FCL leucogranite (Roda-Robles *et al.*, 2009; Vieira, 2010), (ii) apatite U-Pb ages from 314 ± 7 to 288 ± 14 Ma obtained on FCL migmatites and leucogranites (Ferreira *et al.*, 2019), as well as (iii) the emplacement ages for late-D3 muscovite-rich leucogranite intrusions to the southern

Table 2. Summary of the U-Pb geochronological data obtained in this study

Locality	Sample	Age type	Age (Ma)	2σ	2σ uncertainty including long term variance	n	$(^{207}Pb/^{206}Pb)_0$	MSWD
Cassiterite U-Pb dating								
Petalite-rich pegmatites								
Bajoca	-	Intercept	**315**	1	**6**	88	0.87 ± 0.01	1.0
Bajoca	-	Concordia	317	2	6	18	-	1.0
Ramalha	P016	Intercept	**312**	2	**6**	31	0.86 ± 0.02	0.3
Pombal	P018	Intercept	314	1	6	29	1.09 ± 0.7	0.2
Plombal	P018	Concordia	**315**	1	**6**	18	-	0.8
Hinojosa	ALM-2	Intercept	**308**	2	**6**	39	0.85 ± 0.01	1.6
Li-mica-rich pegmatites								
Feli	MF1001c	Intercept	**310**	2	**6**	30	0.85 ± 0.03	0.5
-	P010	Intercept	**313**	2	**6**	27	0.83 ± 0.02	2.2
Ramalha-East	*ALM-3*	*Intercept*	*310*	*24*	*25*	*7*	*0.84 ± 0.01*	*4.6*
Ramalha-West	*P017*	*Intercept*	*312*	*3*	*7*	*18*	*0.86 ± 0.01*	*6.8*
CGM U-Pb dating								
Petalite-rich pegmatite								
Bajoca	MB1001B	Mean $^{206}Pb/^{238}U$	309	3	–	8	–	0.5
Li-mica-rich pegmatite								
Feli	MF1001C	Intercept	308	4	–	15	–	1.2
Feli	MF1001C	Mean $^{206}Pb/^{238}U$	308	3	–	15	–	0.4
Feli	MF1001C	Concordia	308	5	–	15	–	1.0

Data in bold are interpreted as the best representative of pegmatite emplacement ages. Age data in italic have high MSWD values.

border of the FCL complex from 308 ± 3 to 300 ± 2 Ma (zircon U-Pb; Díez Fernández and Pereira 2017; Ferreira *et al.*, 2019). Apatite U-Pb ages were interpreted by Ferreira *et al.* (2019; 2022) as reflecting the exhumation and cooling of the FCL dome below the closure temperature of the apatite U-Pb system between ~485 and 465 °C (Cherniak *et al.*, 1991) in relation with D3 transpressive tectonics. Like apatite, the mica $^{40}Ar/^{39}Ar$ ages may have recorded the cooling of pegmatites below temperatures of ~550-350 °C, corresponding to the closure of muscovite $^{40}Ar/^{39}Ar$ system depending on grain size and cooling rate (Harrison *et al.*, 2009). However, the temperatures of emplacement reported for pegmatite-forming magmas are commonly low, between 550°C and 450°C (London, 2014), and within the range of closure temperatures defined for the muscovite $^{40}Ar/^{39}Ar$ geochronometer. Therefore, a more likely hypothesis to explain the relatively young ages yielded by the mica $^{40}Ar/^{39}Ar$ system within the FA pegmatite field is a partial or complete open-system behavior of this geochronometer during a late-D3 thermal event, in relationship with magmatic pulses marked by the emplacement of late leucogranite intrusions within the FCL complex until 300 ± 2 Ma (Ferreira *et al.*, 2019). Although Pb diffusion data in cassiterite remains scarce, Zhang *et al.* (2011, 2014) have reported relatively high closure temperatures > 500 °C for cassiterite grains. To our knowledge, no closure temperature data are available for the CGM U-Pb system. However, pegmatite geochronology studies based on different isotopic systems generally report mica $^{40}Ar/^{39}Ar$ (and apatite U-Pb) ages significantly younger than CGM and cassiterite U-Pb ages, whereas CGM and cassiterite U-Pb ages are commonly similar to zircon U-Pb ages (*e.g.*, Van Lichtervelde *et al.*, 2017; Li *et al.*, 2019; Hao-Yu *et al.*, 2023). Therefore, the cassiterite and CGM U-Pb systems are much more likely to have recorded the age of emplacement of Li-pegmatites from the FA field compared to mica Ar-Ar ages.

The CGM U-Pb age of 302 ± 3 Ma for a FA Li-mica-rich pegmatite (Roda-Robles *et al.*, 2023) is surprisingly young (despite some overlap with our age data). However, excess variance or long–term reproducibility for CGM U-Pb ages has not been defined yet, meaning that associated uncertainties are likely underestimated. Considering a more realistic uncertainty of ~2% for LA-ICP-MS U-Pb age data (Horstwood *et al.*, 2016; Carr *et al.*, 2023), the error of CGM U-Pb ages obtained for FA pegmatites would be of ± 6 Ma. Therefore, although it is possible that Li-pegmatite-forming magmatism in the FA field was pulsatile over a period from ca. 315 to 302 Ma, all cassiterite and CGM U-Pb ages (*i.e.*, from 315 ± 6 to 302 ± 6 Ma) are almost identical within uncertainty around 310-308 Ma.

Overall, our U-Pb CGM and cassiterite dating suggests that both petalite-rich and Li-mica-rich pegmatite dykes from the FA field were mostly emplaced sub-contemporaneously at the end of the main pulse of leucogranite intrusions and migmatization in the FCL anatectic complex (*i.e.*, within the precision of method). Pegmatite-forming magmatism from 315 ± 6 to 308 ± 6 Ma occurred just after D2 extension and contemporaneously with D3 strike-slip tectonics that affected the leucogranites during and after their crystallization (Fig. 16) (Díez Fernández and Pereira, 2016). Within or close to the FCL anatectic complex, in the sillimanite and andalusite M2 metamorphic zones, pegmatite dykes are commonly barren, variably deformed and strike roughly W-E to WNW-ESE parallel to the S3 foliation of their host-rock. In contrast, pegmatites emplaced at higher structural level, from the

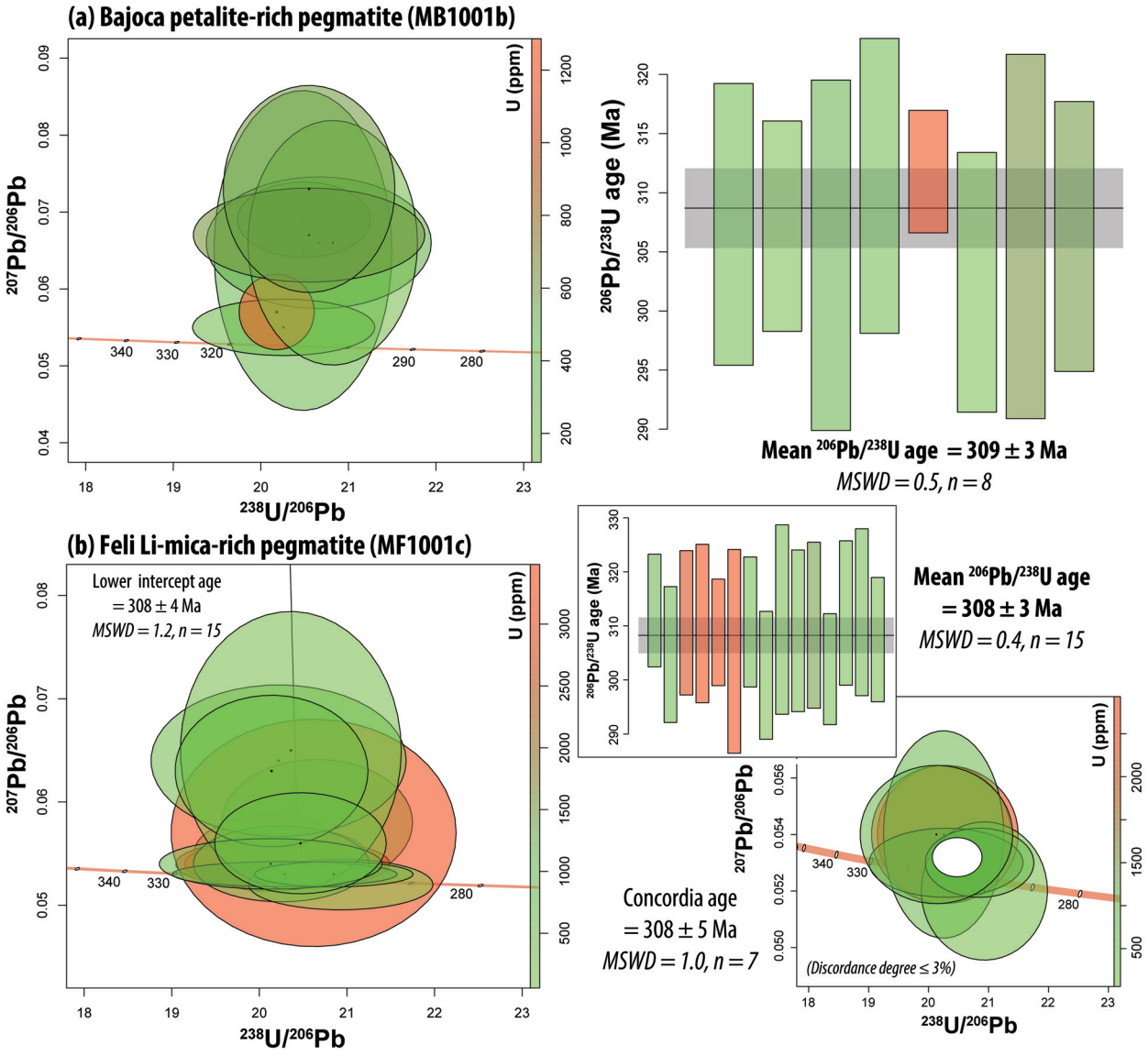

Fig. 15. Tera-Wasserburg and weighted mean $^{206}Pb/^{238}U$ age diagrams for columbite-group minerals from the Bajoca petalite-rich pegmatite (a) and Feli Li-mica-rich pegmatite (b). Ellipses, error bars and ages are reported at 2σ. Colors represent semi-quantitative U concentrations.

andalusite to chlorite M2 zones, have a higher rare-metal potential and commonly strike N10 to N30 perpendicular to the S3 axial plane foliation of metasedimentary rocks (Villar *et al.*, 1990; Vieira *et al.*, 2011) (Fig. 2b). Due to their different orientations, Group 1 barren conformable pegmatites were interpreted as significantly older than discordant Group 2 weakly mineralized and Group 3 Li-Sn-Nb-Ta-mineralized pegmatites (*e.g.*, López Plaza *et al.*, 1982; Ferreira da Silva and Luisa Ribeiro, 1994; Vieira *et al.*, 2011). Such structural relationship is not in conflict with our U-Pb dataset as well as zircon U-Pb ages for leucogranites from the FCL complex (Ferreira *et al.*, 2019), considering the precision of the LA-ICP-MS method (< 2% or ± 6 Ma). However, available U-Pb ages, indeed, suggest that most leucogranites in the FCL complex as well as most pegmatites from the FA field, including barren pegmatites locally intruding FCL leucogranites, were emplaced over a period of about 10 Ma (ca. 317-308 Ma), with possibly a last pulse ca. 302 Ma ago related to late- to post-D3 magmatism (Roda-Robles *et al.*, 2023).

In our view, the various pegmatite orientations over the FA field are, thus, most likely the expression of an evolution of the same D3 strike-slip deformation regime at different structural levels (Figs. 2b and 3). In such sinistral transpressive framework, barren pegmatites in deeper ductile crustal levels would have been mostly emplaced as ~E-W shear veins within the S3 foliations of leucogranites or metasedimentary rocks, whereas in shallower crustal levels, the Li-rich pegmatite-forming magmas would have been dominantly channeled into semi-brittle to brittle fracture networks including mostly ~NNE-SSW tension gashes or locally ENE-WSW Riedel shears oblique to the foliations of metasedimentary rocks (Fig. 2b).

The apparent structural level of emplacement of D3-related pegmatites, marked by M2 metamorphic isograds, evolves toward the north along with their Li fertility (Figs. 2b

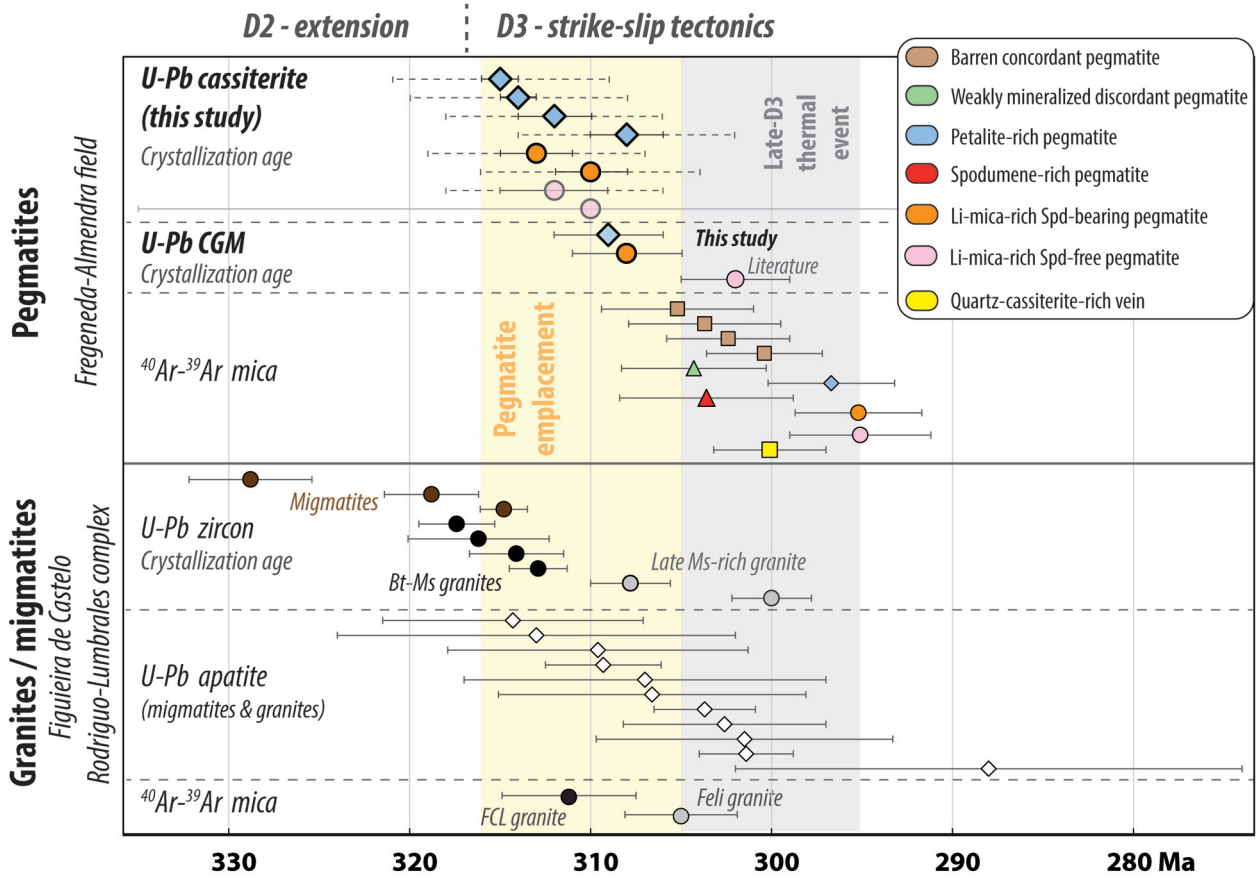

Fig. 16. Summary of geochronological data from the Fregeneda-Almendra pegmatite field and Figueira de Castelo-Lumbrales anatectic complex. Symbols in light colors represent cassiterite U-Pb ages with high MSWD. Errors bars (2σ) in dashed include the long-term variance of cassiterite validation material. The yellow field represents the main emplacement period of pegmatites, and the grey field represents a late-D3 thermal event associated with the emplacement of minor muscovite-rich leucogranite intrusions within the FCL complex. U-Pb zircon and apatite ages are from Ferreira *et al.* (2019, 2022) as well as Díez Fernández and Pereira (2017), and ^{40}Ar-^{39}Ar mica ages are from Roda-Robles *et al.* (2009, 2023) and Vieira (2010). One CGM-U-Pb age is from Roda-Robles *et al.* (2023).

and 3); this could be related to the capacity of vertical migration of their parent melts, largely controlled by their viscosity and relative enrichment in fluxing components such as Li, F, P and H_2O (Bartels *et al.*, 2011; Thomas and Davidson, 2012; Fiege *et al.*, 2018). Indeed, the switch from D2 extension to D3 strike-slip tectonics around 317 Ma was likely a progressive process, between a stress field dominated by gravity forces toward horizontal shortening dominated by tectonic forces, and the orientation of deformation axes have probably not fundamentally changed during this transition (Díez Fernández and Pereira, 2016). That is why, although variably folded during D3 compression, M2 isograds and S0 bedding strike roughly parallel to the contact with the FCL complex and S3 fabrics (Fig. 2). Moreover, as suggested by U-Pb zircon dating of migmatites (Ferreira *et al.*, 2022), peak high temperature-low pressure M2 metamorphism in the FCL complex at 317 ± 2 Ma likely preceded but was not completely disconnected with the beginning of pegmatite-forming magmatism at 315 ± 6 Ma. Thus, we suggest that M2 metamorphic zones, recorded by metasedimentary host-rocks of pegmatites, represent relevant proxies of the vertical distance of migration of the D3-related pegmatite-forming magmas from their sources located in the deeper crust (Fig. 3).

The cassiterite and CGM U-Pb ages of pegmatites from the FA field between 315 ± 6 and 302 ± 6 Ma overlap with CGM U-Pb ages obtained for other LCT pegmatites from the Iberian Massif, ranging from 312 ± 4 to 300 ± 4 Ma, as well as cassiterite or CGM U-Pb ages for LCT pegmatites and peraluminous rare-metal granites from the Armorican Massif and the French Massif Central (Fig. 1) (Gourcerol *et al.*, 2019; Marcoux *et al.*, 2021; Melleton *et al.*, 2022). This confirms that the FA pegmatite field represents the local expression of a major and widespread late-orogenic tectonic-magmatic-metallogenic event occurring at the scale of the European Variscan belt.

8.3 Pegmatite-forming melt evolution as seen through CGM and cassiterite compositions

U-Pb dating of cassiterite and CGM supports a possible link between FA pegmatites and FCL leucogranites and late migmatites. However, the petrogenetic relationship between

those rocks, including different pegmatite types, deserve to be assessed using suitable geochemical tracers. The composition of CGM is widely used as a marker of differentiation in rare-metal pegmatites and granites. Indeed, Mn/Fe and Ta/Nb ratios are known to generally increase in the residual melt during fractional crystallization processes involving micas and/or oxide minerals, as Nb and Fe are more compatible (or less incompatible) than Ta and Mn, respectively (Černý and Ercit, 1985; Linnen and Keppler, 1997; Stepanov *et al.*, 2014; Ballouard *et al.*, 2016, 2020a, 2020b; Garate-Olave *et al.*, 2020). The cassiterite composition as a marker of the magmatic evolution remains unclear, probably because magmatic cassiterite is not as common as CGM in rare-metal granites and pegmatites. Moreover, cassiterite can only accommodate a limited number of elements in its lattice, requiring the use of analytical techniques with low detection limits such as LA-ICP-MS over common electron microprobe analyses, to assess significant compositional variabilities.

Despite a portion of CGM may have crystallized in relation with albitization processes, their Mn-Fe signature appears to be globally inherited from the initial pegmatite-forming melt. Indeed, the Mn* values of discrete CGM from petalite-rich pegmatites evolve consistently with the M2 metamorphic grade of their country-rocks that we suggest as an approximate indicator of the structural levels of emplacement of pegmatites (Fig. 3). Explicitly, CGM from the Bajoca pegmatite emplaced within the andalusite zone have a less evolved geochemical signature, *i.e.,* lower Mn*, than CGM from the Hinojosa and Ramalha pegmatite emplaced at higher structural level within the biotite zone (Fig. 11). In contrast, Ta* variability in the CGM seems to mostly reflect internal evolution processes occurring during pegmatite-forming magma crystallization at the site of emplacement. Tin and Ti concentrations also decrease in CGM from the Bajoca to the Ramalha and Hinojosa petalite-rich pegmatites (Fig. 11b). The decrease of Ti concentrations, an element with a typically compatible behavior in peraluminous granitic melts, likely reflects magma differentiation. The rough correlation between Sn and Ti contents is more difficult to interpret but might reflect the coupled substitution of Ti^{4+} and Sn^{4+} in the structure of CGM.

Similarly, Ti concentrations, along with Ti/Zr and Mn/Fe ratios, appear to change in cassiterite along with the structural level of emplacement of pegmatites, whereas those geochemical parameters have remained globally unchanged during metasomatism, as reflected by low-CL and high-CL cassiterite from the Bajoca pegmatite (Fig. 13). Cassiterite from the Bajoca pegmatite emplaced in the andalousite zone generally has higher Ti contents and Ti/Zr ratios along with lower Mn/Fe ratios than other pegmatites emplaced at higher crustal level in the biotite zone such as the Hinojosa and Ramalha pegmatites. Additionally, cassiterite from the Feli Li-mica-rich pegmatite located in the chlorite zone, at the northern extremity of the FA field, is globally characterized by higher Mn/Fe ratios than that from other pegmatites emplaced in the biotite zone (Figs. 12c and 13).

The evolved signature of cassiterite from the Li-mica-rich and spodumene-bearing Feli pegmatite contrasts with interpretations of Viera *et al.* (2011) based on mica compositions suggesting that this pegmatite subtype is less evolved than Li-mica-rich and spodumene-free subtype (*i.e.*, Ramalha locality). Indeed, muscovite to lepidolite from a Li-mica-rich and spodumene-bearing pegmatite (Viera *et al.*, 2011) have intermediate compositions in terms of Mn-Fe and F systematics between micas from petalite-rich and Li-mica-rich spodumene-free pegmatites (Fig. 8). More samples, coupled with precise estimations of the pressure of pegmatite emplacement, would be needed to reconcile the discrepancies between cassiterite and mica compositions.

In the meantime, available data on CGM and cassiterite are globally consistent with an evolution of their Mn/Fe ratios and Ti compositions in *extrinsic* relationship with the vertical distance of migration of the pegmatite-forming magmas away from their source(s) that may correspond to buried equivalents of rocks, including leucogranites, from the FCL anatectic complex. Such compositional variation in oxide minerals might have occurred in *intrinsic* relationship with the evolution of their parent melts. In such scenario, the most evolved pegmatite-forming magmas, with high Mn/Fe ratios and low Ti concentrations (*i.e.*, crystallizing high Mn/Fe and low Ti oxide minerals), could have emplaced at the highest structural levels because they were also the most enriched in fluxing components that influenced their respective capacities of vertical migration within the crust.

8.4 The petrogenesis of distinct Li-pegmatite types from the Fregeneda-Almendra field as seen through Mn-Fe and F geochemical fractionation

U-Pb geochronology supports the coeval emplacement and possible cogenetic relationship between the distinct types of Li-pegmatites from the FA field including petalite-rich and Li-mica-rich dykes, as suggested by previous studies based notably on micas, phosphate, feldspar and whole-rock compositions (Roda-Robles *et al.*, 1999, 2010, 2023; Vieira *et al.*, 2011). Moreover, cassiterite and CGM from those two pegmatite types show significantly distinct compositions: oxide minerals from Li-mica-rich pegmatites are notably characterized by important enrichment in Mn over Fe, low Ti concentrations and, at least for cassiterite, high Zr and Ga contents, compared to that from petalite-rich pegmatites (Figs. 11, 12 and 13). Such a distinct composition is particularly marked by the Mn* signature of CGM (Fig 11a). Comparisons with CGM and cassiterite data from the literature for the FA pegmatite field (Roda-Robles *et al.*, 1999; Vieira, 2010) (Figs. 11 and 12) confirm this tendency and also indicate that CGM and cassiterite from spodumene-rich pegmatites, weakly mineralized pegmatites and quartz-cassiterite-rich veins have compositions comparable to that from petalite-rich pegmatites.

A similar composition gap in terms of Mn* compositions was observed for CGM between Li-mica-rich pegmatites and petalite/spodumene-rich or weakly mineralized pegmatites from the Barroso-Alvao pegmatite field (Galicia Trás Os Montes Zone of the Iberian Massif), that were emplaced sub-synchronously with FA pegmatites (Martins *et al.*, 2011) (Fig. 1). These authors suggested that this compositional gap might reflect the existence of distinct melt batches, and thus that Li-mica rich pegmatites may not represent a more evolved equivalent of petalite/spodumene-rich pegmatites. However, in the case of the FA field, such compositional gap is partially filled by CGM from a spodumene-bearing Li-mica-rich pegmatite (Vieira, 2010) (Fig. 11a) suggesting that the distinct

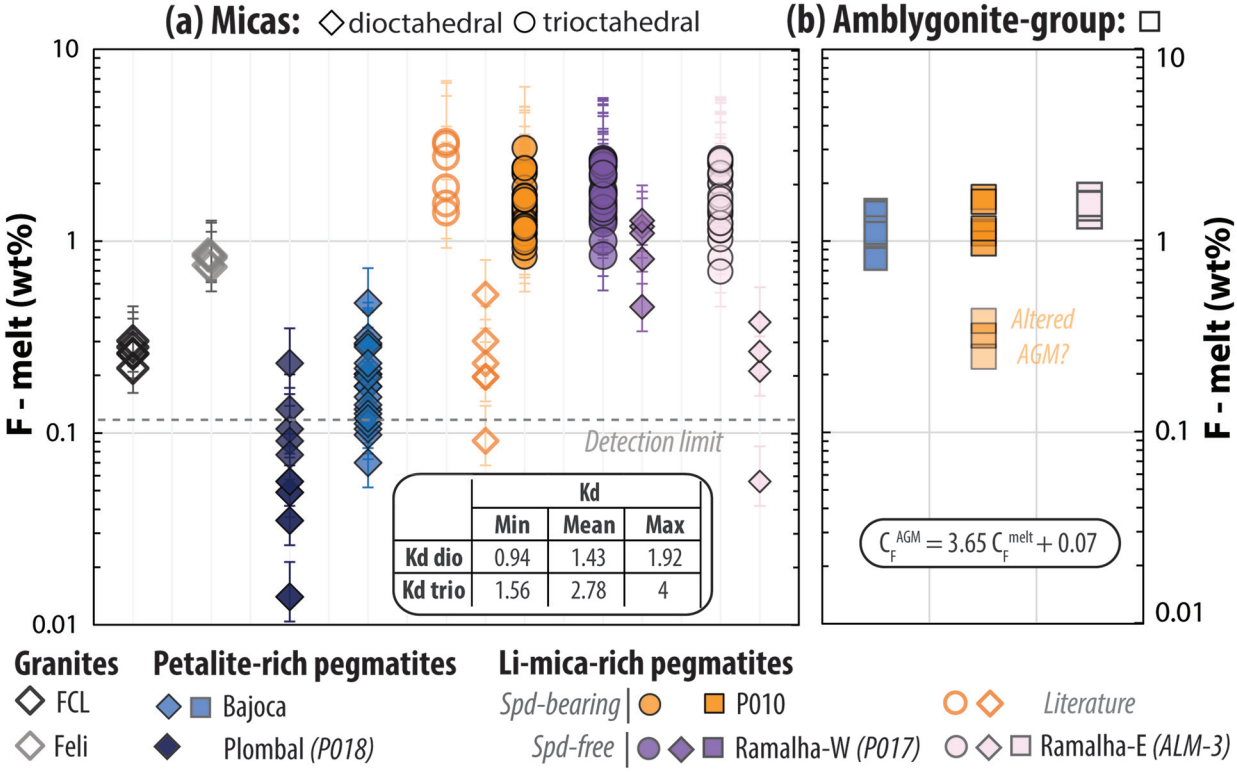

Fig. 17. Calculated F compositions of the melts in equilibrium with micas (a) and amblygonite-group minerals (b) from investigated samples of Li-pegmatites of the FA field (filled symbols). The compositions of the melts equilibrated with micas from regional leucogranites (Figueira de Castelo Rodriguo-Lumbrales – FCL complex and Feli intrusion) and from a Li-mica-rich and spodumene-bearing pegmatite are shown for comparison as empty symbols (data from Vieira, 2010). Mica/granitic melt partitioning coefficients (Kd) correspond to the mean of minimum and maximum values for dioctahedral (muscovite) and trioctahedral (biotite) micas compiled in Villaros and Pichavant (2019) and error bars show the deviation based on the use of min and max Kd values (see inset). We use biotite Kd values for trioctahedral Li-muscovite and lepidolite as no value is available for such mica compositions. The F concentrations of the melts in equilibrium with AGM are calculated using the regression of London *et al.* (2001) (see inset). Low-F AGM in P010 pegmatite are interpreted as altered.

oxide mineral compositions shown by the different Li-pegmatite types could reflect a continuous magmatic evolution. Indeed, strong Mn over Fe enrichment is a common feature of CGM from lepidolite-bearing pegmatites worldwide, and such geochemical fractionation have been interpreted to reflect the high F activity, and more specifically the high alkali-fluorine over HF chemical potential (μalkF/μHF), of their parental melts (Černý, 1989, 1992; Wise *et al.*, 2012). Moreover, F notably increases the solubility of zircon in silicate melts (Keppler, 1993; Aseri *et al.*, 2015), and this may explain the higher concentrations of Zr, and probably Ga, of cassiterite from FA Li-mica-rich pegmatites compared to that from petalite-rich pegmatites (Fig. 13). In the FA field, the high F activity of Li-mica-rich pegmatite-forming magmas, relative to that of petalite-rich muscovite-bearing pegmatites, is at first order suggested by the presence of lepidolite with up to 8 wt% F, also characterized by enrichment of Mn over Fe (Fig. 8), as well as topaz (Fig. 7c) or fluorcalciomicrolite (Fig. 9e) for the Ramalha Li-mica-rich pegmatites. In the Ramalha-E pegmatite, topaz is partially resorbed by lepidolite (Fig. 7c) suggesting a decrease of HF chemical potential, stabilizing lepidolite over topaz (Wise *et al.*, 2012), during magma crystallization.

In the F vs Mn *minus* Fe diagram (Fig. 8), micas from pegmatites of the FA field (data from this study and Vieira *et al.*, 2010), as well as from potential source leucogranites from the FCL complex and buried Feli intrusion (data from Vieira, 2010) do not define chemical trends compatible with a fractional crystallization series. Consistently with the evolution of Mn/Fe ratios of oxide minerals, the Mn – Fe values of micas increase from (i) granites and barren pegmatites, (ii) petalite/spodumene-rich and weakly mineralized pegmatites to (iii) Li-mica-rich pegmatites. Moreover, mica Mn – Fe values anticorrelate with mica Ti contents (not shown). However, the muscovite from weakly mineralized and petalite/spodumene-rich pegmatites, as well as few dioctahedral micas from Li-mica-rich pegmatites, is generally depleted in F ($\leq$ 0.15 apfu) compared to that from granites and barren pegmatites (0.15–0.50 apfu). Such anti-correlation between Mn – Fe and F contents is not consistent with a magmatic evolution process during which F is expected to behave incompatibly and be enriched in the residual liquid.

In order to resolve the discrepancy shown by the F composition of micas, we have calculated in Figure 17a the F concentration of the granitic melts in equilibrium with dioctahedral (muscovite) and trioctahedral (Li-muscovite to

lepidolite) micas from Li-pegmatites of the FA field based on available partition coefficients $Kd_F^{mica/granitic\ melt}$ (Icenhower and London, 1995; Pichavant *et al.*, 2016; Villaros and Pichavant, 2019). The calculated melts in equilibrium with Li-muscovite to lepidolite from Li-mica-rich pegmatites have relatively high F concentrations between ~0.7 and 3.0 wt%, and such composition matches that of the silicate liquid in equilibrium with fresh AGM from those pegmatites (~1–2 wt% F), calculated using the regression of London *et al.* (2001) (Fig. 17b). The F composition of those melts were mostly above that of the silicate liquid equilibrated with muscovite from the Feli leucogranite (0.5–1.3 wt%) considering the uncertainty on partitioning coefficients. However, the liquid equilibrated with muscovite from the petalite-rich pegmatites was strongly depleted in F (<0.1 to ~0.5 wt%) similar to or below that of the melt in equilibrium with the muscovite from the FCL leucogranite (~0.2–0.4 wt%). Those melt compositions contrast with that calculated based on the F concentrations of AGM from the Bajoca-petalite-rich pegmatite that have equilibrated with a significantly enriched melt with 0.8 to 1.5 wt% F.

The compositional differences between the melt in equilibrium with muscovite and AGM for the Bajoca pegmatite likely reflects the depletion in F of the liquid during pegmatite crystallization as AGM is partially resorbed by muscovite in petalite-rich intrusions (Fig. 7a, b). Therefore, AGM are probably early magmatic near-liquidus phases that crystallized from a F-rich melt whereas muscovite might have crystallized near solidus from a F-poor melt that experienced the exsolution of a F-rich fluid (or hydrosaline melt) (Fig. 5). Evidence for such F-rich fluids include the presence of zinnwaldite overgrowths with up to 8 wt% F on muscovite in the Bajoca-pegmatite (Figs. 7a, b and 8), and strong F enrichment from few hundred ppm to up to 0.3 wt% of its metasomatized metasedimentary country-rock (Errandonea-Martin *et al.*, 2022). The modeling presented in Figure 17 suggests that the melt F concentration decreased from ~1.0 to 0.2 wt% between AGM and muscovite crystallization. Therefore, up to 80 wt% of the F budget of the initial melt might have been lost in an immiscible aqueous phase upon crystallization. Amblygonite-group minerals are also partially replaced by Li-muscovite and lepidolite in Li-mica-rich pegmatites (Fig. 7d) but both crystallized from a F-rich melt with ~1–3 wt% F (Fig. 17). This indicates that F was mostly trapped in trioctahedral micas before melt-fluid (or silicate melt-hydrosaline melt) immiscibility and exsolution, although metasomatism involving aqueous media is notably recorded by strong F enrichment in Li-mica-rich pegmatite country-rocks (up to 0.7 wt%, Errandonea-Martin *et al.*, 2022).

The fact that the initial melt composition of petalite-rich pegmatites exhibits only slightly lower F concentrations (≤ ~1.5 wt%), although not significantly different from those of Li-mica-rich pegmatite-forming melts (≤ ~2 wt%), suggests that lepidolite stability is influenced not solely by the magma F content, but also by other physicochemical parameters. Relatively high oxygen fugacity, between ~NNO+3 and NNO+1, is a prerequisite to crystallize Li-micas, or muscovite, relative to biotite in granitic magmas as suggested by crystallization experiments (Pichavant *et al.*, 2016; Pichavant, 2022). However, neither petalite-rich nor Li-mica-rich pegmatites host magmatic biotite, but both contain early cassiterite with likely magmatic origin, suggesting that the parental melts of both pegmatite types were characterized by similarly high fO_2. Alternatively, the pressure of magma emplacement might have played a significant role for lepidolite crystallization as Li-mica-rich pegmatites were globally emplaced at higher structural levels than petalite-rich pegmatites (Figs. 2 and 3). The pressure could have directly affected the stability of lepidolite or more likely affected the water concentration of the melt, as H_2O solubility is known to increase with pressure. The decrease of H_2O/F melt activity ratio, or more precisely $\mu HF/\mu alkF$ as suggested by Wise *et al.* (2012), from petalite- to Li-mica-rich pegmatites was possibly the trigger for lepidolite (and Li-muscovite) crystallization. Experimental work would be needed to confirm this hypothesis.

Overall, oxide mineral, phosphate and mica compositions along with CGM and cassiterite U-Pb geochronology support a cogenetic relationship between petalite-rich and Li-mica-rich pegmatites. In such a framework, the Mn/Fe and Ti compositions of minerals suggest that Li-mica-rich pegmatites represent a more differentiated equivalent of petalite-rich pegmatites, as suggested by previous studies (*e.g.*, Vieira *et al.*, 2011; Roda-Robles *et al.*, 2023). The F composition of the initial melts of both pegmatite types was relatively similar although probably slightly higher in Li-mica-rich pegmatites. U-Pb geochronology and mineralogical-chemical zonation of the pegmatite field suggests that the source of pegmatites could correspond to buried equivalents of rocks from the FCL complex. Our data do not allow to favor either a residual or anatectic origin for Li-pegmatites as the timing of their emplacement overlaps with the zircon crystallization ages of both migmatites and granites in the complex (Fig. 16). Equivalents of the leucogranite intrusion located below the Feli mine could have represented fertile parent magmas, notably considering the high F concentration of Feli granite muscovite (data from Vieira, 2010) (Fig. 17). However, without zircon U-Pb dating, the potential relationship between such evolved leucogranite intrusions and Li-pegmatites remains uncertain.

9 Conclusions and implications

U-Pb dating of cassiterite and CGM from pegmatites from the FA field demonstrates the sub-coeval emplacement of two main types of Li-Sn-Nb-Ta-rich pegmatite intrusions, including Li-mica-rich and petalite-rich pegmatites, in relation with D3-strike-slip tectonics from ca. 315 to 308 Ma (Fig. 16). A late pulse of Li-pegmatite-forming magmatism possibly occurred ca. 302 Ma ago (Roda-Robles *et al.*, 2023). Several other Li-pegmatite fields from Iberia were also emplaced during this period (Melleton *et al.*, 2022) (Fig. 1), supporting late-orogenic transcurrent tectonic framework as a particularly favorable context for the emplacement of rare-metal pegmatite intrusions. Indeed, such context likely favors the generation of the vertical dilation structures (*e.g.*, tension gashes) necessary for flux-rich magma ascent. Intimate relationship between strike-slip tectonics and peraluminous rare-metal magmatism is also documented, for example, in the Argemela area, Iberian belt (Michaud *et al.*, 2020) (Fig. 1), the Variscan Echassières district, French Massif Central (Gagny and Jacquot, 1987) (Fig. 1), the Neoproterozoic Seridó belt, Brazil (Araújo *et al.*,

2001) and the Mesoproterozoic Orange River pegmatite belt, South Africa (Ballouard *et al.*, 2020a).

The geographic zonation of pegmatite around the FCL anatectic dome and U-Pb geochronology suggest a genetic link between buried equivalents of ca. 317-313 Ma old leucogranites (or migmatites) from the dome and FA rare-metal magmatism. Cassiterite, CGM and micas show decreasing Ti contents as well as increasing Mn/Fe ratios and Zr-Ga contents (for oxide minerals) from petalite- to Li-mica-rich pegmatites. This is consistent with a magmatic differentiation process, notably leading to an increase of the F activity of parental melts. Geochemical analyses of coexisting phosphates and micas suggest a decrease of F melt concentrations from $\leq$ 1.5 to $<$ 0.5 wt% between near-liquidus AGM and near-solidus muscovite crystallizations in petalite-rich pegmatites. Most of the initial F melt budget may have been lost to an aqueous phase during the magmatic-hydrothermal transition. Late circulation of F-rich fluids is reflected by the local occurrence of zinnwaldite overgrowths on muscovite, and strong enrichment in F of pegmatite country-rocks (Errandonea-Martin *et al.*, 2022). The melts equilibrated with AGM and Li-muscovite to lepidolite in Li-mica-rich pegmatites had similarly high F concentration $\leq$ ~2–3 wt% indicating that F was largely trapped in Li-micas before the magmatic-hydrothermal transition. Relatively similar F concentrations in the initial melt of both petalite- and Li-mica-rich pegmatites support the hypothesis that lepidolite stability depends not on only on F activity but also on other parameters such as a relatively low H_2O activity (μHF) relative to alkaline-fluorine salinity (μalkF), as previously suggested by Wise *et al.* (2012). We tentatively propose that the lower H_2O activity in the melt of Li-mica-rich pegmatites from the FA field, compared to that of petalite-rich pegmatites, was due to a lower pressure of emplacement that could have decreased water solubility.

Supplementary Material

Figure S1. – Summary of U-Pb ages obitained for the Jian-1 cassiterite in the course of the diffrent LA-ICP-MS analytical session during which the cassiterite crystal from the Fregeneda-Almendra pegmatite field were analyzed. The recommended age of the Jian-1 cassiterite is 154.97 ± 0.08 Ma.

The Supplementary Material is available at https://www.bsgf.fr/10.1051/bsgf/2023015/olm.

Acknowledgment. The post-doctoral fellowship of C. Ballouard was supported by the French National Research Agency through the national program 'Investissements d'avenir' with the reference ANR-10-LABX-21-RESSOURCES21, the Grand Est region *via* the program 'Jeunes chercheurs' 2020 (19_GE9_066) and the ANR TRANSFAIR (ANR-21-CE01-0022-01). The Master's thesis of F. Parisot was funded by the ANR-10-LABX-21-RESSOURCES21 program. Additional funding was provided by the ERA-MIN/0001/2017–LIGHTS project. The LA-ICP-MS laboratory of GeoRessources in Nancy was funded by the Labex Resources 21, the Région Lorraine and the European Community through the FEDER program. R. Schmitt participated to the sampling and provided some field photographs. We acknowledge E. Roda-Robles and A. Lima for discussions and support during sampling. We are grateful to E. Moreira for her help during LA-ICP-MS analyses as well as to A. Petrelli for LIGHTS project management. A. Flammang and J. Moine are thanked for thick section preparation. Earlier versions of this manuscript benefited from the scientific comments of M. Sirbescu, J. Cempírek, A. Acosta-Vigil and one anonymous reviewer. We thank M. Van Lichtervelde and one anonymous reviewer for their comments on the present version, and we are grateful to M. Poujol for editorial handling.

References

Ábalos B, Carreras J, Druguet E, *et al.* 2002. Variscan and pre-Variscan tectonics. In Gibbons W, Moreno T, eds.Geol. Spain, pp. 155-183.

Antunes IMHR, Neiva AMR, Ramos JMF, Silva PB, Silva MMVG, Corfu F. 2013. Petrogenetic links between lepidolite-subtype aplite-pegmatite, aplite veins and associated granites at Segura (central Portugal). *Chemie der Erde* 73: 323–341.

Araújo MNC, da Silva FCA, de Sá EFJ. 2001. Pegmatite emplacement in the Seridó Belt, northeastern Brazil: late stage kinematics of the Brasiliano orogen. *Gondwana Res* 4: 75–85.

Aseri AA, Linnen RL, Che XD, Thibault Y, Holtz F. 2015. Effects of fluorine on the solubilities of Nb, Ta, Zr and Hf minerals in highly fluxed water-saturated haplogranitic melts. *Ore Geol Rev* 64: 736–746.

Ballèvre M, Catalán JRM, López-Carmona A, *et al.* 2014. Correlation of the nappe stack in the Ibero-Armorican arc across the Bay of Biscay: a joint French-Spanish project. *Geol Soc London, Spec Publ* 405: 77–113.

Ballèvre M. 2016. Une histoire géologique du Massif armoricain. *Géochronique* 140.

Ballèvre M, Bosse V, Ducassou C, Pitra P. 2009. Palaeozoic history of the Armorican Massif: models for the tectonic evolution of the suture zones. *Comptes Rendus Geosci* 341: 174–201.

Ballouard C, Poujol M, Boulvais P, Branquet Y, Tartèse R, Vigneresse JL. 2016. Nb-Ta fractionation in peraluminous granites: a marker of the magmatic-hydrothermal transition. *Geology* 44: 231–234.

Ballouard C, Elburg MA, Tappe S, Reinke C, Ueckermann H, Doggart S. 2020a. Magmatic-hydrothermal evolution of rare metal pegmatites from the Mesoproterozoic Orange River pegmatite belt (Namaqualand, South Africa). *Ore Geol Rev* 116: 103252.

Ballouard C, Massuyeau M, Elburg MA, Tappe S, Viljoen F, Brandenburg JT. 2020b. The magmatic and magmatic-hydrothermal evolution of felsic igneous rocks as seen through Nb-Ta geochemical fractionation, with implications for the origins of rare-metal mineralizations. *Earth-Sci Rev* 203: 103115.

Ballouard C, Couzinié S, Bouilhol P, Harlaux M, Mercadier J, Montel JM. 2023. A felsic meta-igneous source for Li-F-rich peraluminous granites: insights from the Variscan Velay dome (French Massif Central) and implications for rare-metal magmatism. *Contrib Mineral Petrol* 178: 75.

Barbarin B. 1999. A review of the relationships between granitoid types, their origins and their geodynamic environments. *Lithos* 46: 605–626.

Bartels A, Vetere F, Holtz F, Behrens H, Linnen RL. 2011. Viscosity of flux-rich pegmatitic melts. *Contrib Mineral Petrol* 162: 51–60.

Bhalla P, Holtz F, Linnen RL, Behrens H. 2005. Solubility of cassiterite in evolved granitic melts: effect of T, fO_2, and additional volatiles. *Lithos* 80: 387–400.

Bonzi WME, Vanderhaeghe O, Van Lichtervelde M, *et al.* 2021. Petrogenetic links between rare metal-bearing pegmatites and TTG gneisses in the West African Craton: the Mangodara district of SW Burkina Faso. *Precambrian Res* 364.

Carnicero MA. 1982. Estudio del metamorfismo existente en torno al granito de Lumbrales (Salamanca). *Stud Geológica Salmant* 17: 7–20.

Carr PA, Moreira E, Neymark L, Norman MD, Mercadier J. 2023. A LA-ICP-MS comparison of reference materials used in cassiterite U-Pb geochronology. *Geostand Geoanalytical Res* 47: 67–87.

Carr PA, Zink S, Bennett VC, Norman MD, Amelin Y, Blevin PL. 2020. A new method for U-Pb geochronology of cassiterite by ID-TIMS applied to the mole granite polymetallic system, eastern Australia. *Chem Geol* 539: 119539.

Černý P. 1989. Contrasting geochemistry of two pegmatite fields in Manitoba: products of juvenile aphebian crust and polycyclic archean evolution. *Precambrian Res* 45: 215–234.

Černý P. 1991. Rare-element granitic pegmatites. Part II: regional to global environments and petrogenesis. *Geosci Canada* 18: 68–81.

Černý P. 1992. Geochemical and petrogenetic features of mineralization in rare-element granitic pegmatites in the light of current research. *Appl Geochemistry* 7: 393–416.

Černý P, Ercit TS. 1985. Some recent advances in the mineralogy and geochemistry of Nb and Ta in rare-element granitic pegmatites. *Bull Minéralogie* 108: 499–532.

Černý P, Ercit TS. 2005. The classification of granitic pegmatites revisited. *Can Mineral* 43: 2005–2026.

Černý P, Meintzer RE, Anderson AJ. 1985. Extreme fractionation in rare-element granitic pegmatites; selected examples of data and mechanisms. *Can Mineral* 23: 381–421.

Chantraine J, Autran J, Cavelier C. 2003. Carte géologique de la France à 1/1 000 000, 6ème édition révisée. BRGM.

Chauvet A, Volland-Tuduri N, Lerouge C, *et al.* 2012. Geochronological and geochemical characterization of magmatic-hydrothermal events within the Southern Variscan external domain (Cévennes area, France). *Int J Earth Sci* 101: 69–86.

Cheilletz A, Archibald DA, Cuney M, Charoy B. 1992. Ages $^{40}Ar/^{39}Ar$ du leucogranite à topaze-lépidolite de Beauvoir et des pegmatites sodolithiques de Chédeville (Nord du Massif Central, France). Signification pétrologique et géodynamique. *Comptes Rendus l'Académie des Sci Série 2, Mécanique, Phys Chim Sci. l'univers, Sci la Terre* 315: 329–336.

Cherniak DJ, Lanford WA, Ryerson FJ. 1991. Lead diffusion in apatite and zircon using ion implantation and Rutherford Backscattering techniques. *Geochim Cosmochim Acta* 55: 1663–1673.

Cuney M, Marignac C, Weisbrod A. 1992. The beauvoir topaz-lepidolite albite granite (Massif Central, France); the disseminated magmatic Sn-Li-Ta-Nb-Be mineralization. *Econ Geol* 87: 1766–1794.

Cuney M, Alexandrov P, Le Carlier de Veslud C, *et al.* 2002. The timing of W-Sn-rare metals mineral deposit formation in the Western Variscan chain in their orogenic setting: the case of the Limousin area (Massif Central, France). *Geol Soc London, Spec Publ* 204: 213–228.

Dallmeyer RD., Garcia EM. 2012. Pre-mesozoic geology of Iberia.

Dallmeyer RD, Martínez Catalán JR, Arenas R, *et al.* 1997. Diachronous Variscan tectonothermal activity in the NW Iberian Massif: evidence from $^{40}Ar/^{39}Ar$ dating of regional fabrics. *Tectonophysics* 277: 307–337.

da Silva AF, dos Santos AJ, Ribeiro A, Ribeiro L. 1991a. Carta Geológica de Portugal na escala 1:50.000. Folha 15A. Vila Nova de Foz Côa. Serviços Geológicos de Portugal.

da Silva AF, dos Santos AJ, Ribeiro A, Cabral J, Ribeiro L. 1991b. Carta Geológica de Portugal na escala 1:50.000. Folha 15B. Freixo de Espada à Cinta. Serviços geológicos de Portugal.

Demartis M, Pinotti LP, Coniglio JE, *et al.* 2011. Ascent and emplacement of pegmatitic melts in a major reverse shear zone (Sierras de Córdoba, Argentina). *J Struct Geol* 33: 1334–1346.

Deveaud S, Gumiaux C, Gloaguen E, Branquet Y. 2013. Spatial statistical analysis applied to rare-element LCT-type pegmatite felds: an original approach to constrain faults-pegmatites-granites relationships. *J Geosci* 58: 163–182.

Deveaud S, Millot R, Villaros A. 2015. The genesis of LCT-type granitic pegmatites, as illustrated by lithium isotopes in micas. *Chem Geol* 411: 97–111.

Dewaele S, Henjes-Kunst F, Melcher F, *et al.* 2011. Late Neoproterozoic overprinting of the cassiterite and columbite-tantalite bearing pegmatites of the Gatumba area, Rwanda (Central Africa). *J African Earth Sci* 61: 10–26.

Dias da Silva ÍF. 2013. Geología de las zonas Centro Ibérica y Galicia-Trás-os-Montes en la parte oriental del Complejo de Morais, Portugal/España. PhD thesis. Universidad de Salamanca.

Dias da Silva Í, Gómez-Barreiro J, Martínez Catalán JR., Ayarza P, Pohl J, Martínez E. 2017. Structural and microstructural analysis of the Retortillo Syncline (Variscan belt, Central Iberia). Implications for the Central Iberian Orocline. *Tectonophysics* 717: 99–115.

Díez Fernández R, Pereira MF. 2016. Extensional orogenic collapse captured by strike-slip tectonics: Constraints from structural geology and U-Pb geochronology of the Pinhel shear zone (Variscan orogen, Iberian Massif). *Tectonophysics* 691: 290–310.

Díez Fernández R, Pereira MF. 2017. Strike-slip shear zones of the Iberian Massif: are they coeval? *Lithosphere* 9: 726–744.

Diez Montes A, Escuder J, Carrasco RM, Rodríguez Fernández LR. 1991. Mapa Geológico de España. Escala 1:50.000. Vilvestre 448–449.

Errandonea-Martin J, Garate-Olave I, Roda-Robles E, *et al.* 2022. Metasomatic effect of Li-bearing aplite-pegmatites on psammitic and pelitic metasediments: geochemical constraints on critical raw material exploration at the Fregeneda-Almendra Pegmatite Field (Spain and Portugal). *Ore Geol Rev* 150: 105155.

Ferreira da Silva A., dos Santos AJ, Ribeiro A, Cabral J, Ribeiro L. 1990a. Carta Geológica de Portugal na escala 1:50.000. Folha 15B. Freixo de Espada à Cinta.

Ferreira da Silva A, dos Santos AJ, Ribeiro A,Ribeiro L. 1990b. Carta Geológica de Portugal na escala 1:50.000. Folha 15A. Vila Nova de Foz Côa.

Ferreira da Silva A, Luisa Ribeiro M. 1994. Notícia explicativa da folha 15B. Freixo de Espada à Cinta—da carta Geológica de Portugal na escala 1:50.000.

Ferreira JA, Bento dos Santos T, Pereira I, Mata J. 2019. Tectonically assisted exhumation and cooling of Variscan granites in an anatectic complex of the Central Iberian Zone, Portugal: constraints from LA-ICP-MS zircon and apatite U-Pb ages. *Int J Earth Sci* 108: 2153–2175.

Ferreira JA, Mata J, Bento dos Santos T, Pereira I. 2020. The role of melting on the geochemical evolution and isotopic variability of an anatectic complex in the Iberian Variscides. *Lithos* 378-379: 105769.

Ferreira JA, Pereira I, dos Santos T, Mata J. 2022. U-Pb age constraints on the protolith, cooling and exhumation of a Variscan middle crust migmatite complex from the Central Iberian Zone: insights into the Variscan metamorphic evolution and Ediacaran palaeogeographic implications. *J Geol Soc London* 179: 2021–072.

Fiege A, Simon A, Linsler SA, Bartels A, Linnen RL. 2018. Experimental constraints on the effect of phosphorous and boron on Nb and Ta ore formation. *Ore Geol Rev* 94: 383–395.

Fosso Tchunte P, Tchameni R, André-Mayer AS *et al*. 2018. Evidence for Nb-Ta occurrences in the syn-tectonic Pan-African Mayo Salah leucogranite (northern Cameroon): constraints from Nb-Ta oxide mineralogy, geochemistry and U-Pb LA-ICP-MS geochronology on columbite and monazite. *Minerals* 8: 188.

Gagny C, Jacquot T. 1987. Contribution de la pétrologie structurale à la connaissance des conditions de mise en place et de structuration complexe du granite des Colettes (Massif d'Echassières, Massif central français). *Géologie la Fr.* 2-3: 47–56.

Garate-Olave I, Roda-Robles E, Gil-Crespo PP, Pesquera A, Errandonea-Martin J. 2020. The tres arroyos granitic aplite-pegmatite field (Central Iberian Zone, Spain): Petrogenetic constraints from evolution of Nb-Ta-Sn oxides, whole-rock geochemistry and U-Pb geochronology. *Minerals* 10: 1–26.

García-Arias M, Díez-Montes A, Villaseca C, Blanco-Quintero IF. 2018. The Cambro-Ordovician Ollo de Sapo magmatism in the Iberian Massif and its Variscan evolution: a review. *Earth-Sci Rev.* 176: 345–372.

Gourcerol B, Gloaguen E, Melleton J, Tuduri J, Galiegue X. 2019. Re-assessing the European lithium resource potential – A review of hard-rock resources and metallogeny. *Ore Geol Rev* 109: 494–519.

Gutiérrez-Alonso G, Fernández-Suárez J, Jeffries TE, *et al.* 2011. Diachronous post-orogenic magmatism within a developing orocline in Iberia, European Variscides. *Tectonics* 30: T C5008.

Gutiérrez-Alonso G, Fernández-Suárez J, López-Carmona A, Gärtner A. 2018. Exhuming a cold case: the early granodiorites of the northwest Iberian Variscan belt-A Visean magmatic flare-up? *Litosphere* 10: 194–216.

Hao-Yu W, Yong T, Hui Z, Zheng-Hang L, Yu-Sheng X. 2023. The geochronology of the rare metal pegmatite deposits: A case study in Nanping No. 31 pegmatite vein in northeastern Cathaysian block, China. *Ore Geol Rev* 153: 105280.

Harrison TM, Célérier J, Aikman AB, Hermann J, Heizler MT. 2009. Diffusion of ^{40}Ar in muscovite. *Geochim Cosmochim Acta* 73: 1039–1051.

Horstwood MSA., Košler J, Gehrels G, *et al.* 2016. Community-derived standards for LA-ICP-MS U-(Th-)Pb geochronology – uncertainty propagation, age interpretation and data reporting. *Geostand Geoanalytical Res* 40: 311–332.

Hulsbosch N, Hertogen J, Dewaele S, André L, Muchez P. 2014. Alkali metal and rare earth element evolution of rock-forming minerals from the Gatumba area pegmatites (Rwanda): Quantitative assessment of crystal-melt fractionation in the regional zonation of pegmatite groups. *Geochim Cosmochim Acta* 132: 349–374.

Icenhower J, London D. 1995. An experimental study of element partitioning among biotite, muscovite, and coexisting peraluminous silicic melt at 200 MPa (H_2O). *Am Mineral* 80: 1229–1251.

Jackson SE, Pearson NJ, Griffin WL, Belousova EA. 2004. The application of laser ablation-inductively coupled plasma-mass spectrometry to *in situ* U-Pb zircon geochronology. *Chem Geol* 211: 47–69.

Kaeter D, Barros R, Menuge JF, Chew DM. 2018. The magmatic-hydrothermal transition in rare-element pegmatites from southeast Ireland: LA-ICP-MS chemical mapping of muscovite and columbite-tantalite. *Geochim Cosmochim Acta* 240: 98–130.

Keppler H. 1993. Influence of fluorine on the enrichment of high field strength trace elements in granitic rocks. *Contrib Mineral Petrol* 114: 479–488.

Knoll T, Schuster R, Huet B, *et al.* 2018. Spodumene pegmatites and related leucogranites from the Austroalpine unit (Eastern Alps, Central Europe): field relations, petrography, geochemistry, and geochronology. *Can Mineral* 56: 489–528.

Knoll T, Huet B, Schuster R, Mali H, Ntaflos T, Hauzenberger C. 2023. Lithium pegmatite of anatectic origin-a case study from the Austroalpine Unit Pegmatite Province (Eastern European Alps): geological data and geochemical model. *Ore Geol Rev* 154: 105298.

Konzett J, Hauzenberger C, Ludwig T, Stalder R. 2018a. Anatectic granitic pegmatites from the Eastern Alps: A case of variable rare metal enrichment during high-grade regional metamorphism. II: Pegmatite staurolite as an indicator of anatectic pegmatite parent melt formation – a field and experimental study. *Can Mineral* 56: 603–624.

Konzett J, Schneider T, Nedyalkova L, *et al.* 2018b. Anatectic granitic pegmatites from the Eastern Alps: A case of variable rare-metal enrichment during high-grade regional metamorphism – I: Mineral assemblages, geochemical characteristics, and emplacement ages. *Can Mineral* 56: 555–602.

Kroner U, Romer RL. 2013. Two plates – many subduction zones: the Variscan orogeny reconsidered. *Gondwana Res* 24: 298–329.

Legros H, Mercadier J, Villeneuve J *et al.* 2019. U-Pb isotopic dating of columbite-tantalite minerals: Development of reference materials and in situ applications by ion microprobe. *Chem Geol* 512: 69–84.

Li P, Li J, Chou IM, Wang D, Xiong X. 2019. Mineralization epochs of granitic rare-metal pegmatite deposits in the songpan-ganzê orogenic belt and their implications for orogeny. *Minerals* 9: 1–25.

Linnen RL, Cuney M. 2005. Granite-related rare-element deposits and experimental constraints on Ta-Nb-W-Sn-Zr-Hf mineralization in Linnen RL Samson IM, eds., rare-element geochemistry and mineral deposits. Geol Assoc Canada, GAC, Short Course.

Linnen RL, Keppler H. 1997. Columbite solubility in granitic melts: consequences for the enrichment and fractionation of Nb and Ta in the Earth's crust. *Contrib Mineral Petrol* 128: 213–227.

Linnen RL, Pichavant M, Holtz F. 1996. The combined effects of fO_2 and melt composition on SnO_2 solubility and tin diffusivity in haplogranitic melts. *Geochim Cosmochim Acta* 60: 4965–4976.

Linnen RL, Van Lichtervelde M, Černý P. 2012. Granitic pegmatites as sources of strategic metals. *Elements* 8: 275–280.

London D. 2014. A petrologic assessment of internal zonation in granitic pegmatites. *Lithos* 184-187: 74–104.

London D. 2018. Ore-forming processes within granitic pegmatites. *Ore Geol Rev* 101: 349–383.

London D, Burt DM. 1982. Alteration of spodumene, montebrasite and lithiophilite in pegmatites of the White Picacho District, Arizona. *Am Mineral* 67: 97–113.

London D, Morgan VIGB, Wolf MB. 2001. Amblygonite-montebrasite solid solutions as monitors of fluorine in evolved granitic and pegmatitic melts. *Am Mineral* 86: 225–233.

López Plaza M, Carnicero Gómez A, Gonzalo Corral JC, *et al.* 1982. Estudio geológico del campo filoniano de La Fregeneda (Salamanca). *Stud Geol Salmant* 17: 89–98.

Marcoux E, Barré B, Pichavant M, Poujol M. 2021. Âge et genèse de la coupole granitique à métaux rares (Sn, Li, Nb-Ta, W) de Montebras (Creuse, Massif central français). *BSGF-Earth Sci Bull* 192: 16.

Martínez Catalán JR., Rubio Pascual FJ, Díez Montes A, *et al.* 2014. The late Variscan HT/LP metamorphic event in NW and Central Iberia: relationships to crustal thickening, extension, orocline development and crustal evolution. *Geol Soc London, Spec Publ* 405: 225–247.

Martínez Catalán JR., Schulmann K, Ghienne JF. 2021. The Mid-Variscan Allochthon: Keys from correlation, partial retrodeformation and plate-tectonic reconstruction to unlock the geometry of a non-cylindrical belt. *Earth-Sci Rev.* 220: 103700

Martins T, Lima A, Simmons WB, Falster AU, Noronha F. 2011. Geochemical fractionation of Nb-Ta oxides in Li-bearing pegmatites from the Barroso-Alvão pegmatite field, northern Portugal. *Can Mineral* 49: 777–791.

Matte P. 1991. Accretionary history and crustal evolution of the Variscan belt in Western Europe. *Tectonophysics* 196: 309–337.

Melcher F, Sitnikova MA, Graupner T *et al.* 2008. Fingerprinting of conflict minerals: columbite-tantalite ("coltan") ores. *SGA News* 23: 7–14.

Melleton J, Gloaguen E, Frei D, Lima A, Vieira R, Martins T. 2022. Polyphased rare-element magmatism during late orogenic evolution: geochronological constraints from NW Variscan Iberia. *BSGF – Earth Sci Bull* 193: 28.

Melleton J, Gloaguen E, Frei D, Novák M, Breiter K. 2012. How are the emplacement of rare-element pegmatites, regional metamorphism and magmatism interrelated in the Moldanubian domain of the Variscan Bohemian Massif, Czech Republic? *Can Mineral* 50: 1751–1773.

Michaud JAS, Gumiaux C, Pichavant M, Gloaguen E, Marcoux E. 2020. From magmatic to hydrothermal Sn-Li-(Nb-Ta-W) mineralization: The Argemela area (central Portugal). *Ore Geol Rev* 116: 103215.

Müller A, Romer RL, Pedersen RB. 2017. The Sveconorwegian pegmatite province – thousands of pegmatites without parental granites. *Can Mineral* 55: 283–315.

Müller A, Spratt J, Thomas R, Williamson BJ, Seltmann R. 2018. Alkali-F-rich albite zones in evolved NYF pegmatites: The product of melt-melt immiscibility. *Can Mineral* 56: 657–687.

Nasdala L, Corfu F, Valley JW, *et al.* 2016. Zircon M127-A homogeneous reference material for SIMS U-Pb geochronology combined with hafnium, oxygen and, potentially, lithium isotope analysis. *Geostand Geoanalytical Res* 40: 457–475.

Neiva AMR, Ramos JMF. 2010. Geochemistry of granitic aplite-pegmatite sills and petrogenetic links with granites, Guarda-Belmonte area, central Portugal. *Eur J Mineral* 22: 837–854.

Pereira I, Dias R, dos Santos TB, Mata J. 2017. Exhumation of a migmatite complex along a transpressive shear zone: inferences from the Variscan Juzbado-Penalva do Castelo Shear Zone (Central Iberian Zone). *J Geol Soc London* 174: 1004–1018.

Pichavant M. 2022. Experimental crystallization of the Beauvoir granite as a model for the evolution of Variscan rare metal magmas. *J Petrol* 63: egac 120.

Pichavant M, Herrera JV, Boulmier S, *et al.* 1987. The Macusani glasses, SE Peru: evidence of chemical fractionation in peraluminous magmas. *Magmat Process Physicochem Princ Geochem Soc Spec Publ* 1: 359–373.

Pichavant M, Villaros A, Deveaud S, Scaillet B, Lahlafi M. 2016. The influence of redox state on mica crystallization in leucogranitic and pegmatitic liquids. *Can Mineral* 54: 559–581.

Raimbault L, Burnol L. 1998. The Richemont rhyolite dyke, Massif Central, France; a subvolcanic equivalent of rare-metal granites. *Can Mineral* 36: 265–282.

Ribeiro ML, Castro A, Almeida A. 2019. Variscan magmatism. In: *The geology of Iberia: a geodynamic approach*. pp. 497-526.

Roda-Robles E, Pesquera Perez A, Velasco Roldan F, Fontan F. 1999. The granitic pegmatites of the Fregeneda area (Salamanca, Spain); characteristics and petrogenesis. *Mineral Mag* 63: 535–558.

Roda-Robles E, Vieira R, Lima A, Pesquera-Pérez A. 2009. Petrogenetic links between granites and pegmatites in the Fregeneda-Almendra area (Salamanca, Spain and Guarda, Portugal): new insights from $^{40}Ar/^{39}Ar$ dating in micas. *Estud Geológicos* 19: 305–310.

Roda-Robles E, Vieira R, Pesquera A, Lima A. 2010. Chemical variations and significance of phosphates from the Fregeneda-Almendra pegmatite field, Central Iberian Zone (Spain and Portugal). *Mineral Petrol* 100: 23–34.

Roda-Robles E, Pesquera A, Gil-Crespo PP, *et al.* 2016. Geology and mineralogy of Li mineralization in the Central Iberian Zone (Spain and Portugal). *Mineral Mag* 80: 103–126.

Roda-Robles E, Villaseca C, Pesquera A, *et al.* 2018. Petrogenetic relationships between Variscan granitoids and Li-(F-P)-rich aplite-pegmatites in the Central Iberian Zone: geological and geochemical constraints and implications for other regions from the European Variscides. *Ore Geol Rev* 95: 408–430.

Roda-Robles E, Vieira R, Lima A, *et al.* 2023. Li-rich pegmatites and related peraluminous granites of the Fregeneda-Almendra field (Spain-Portugal): a case study of magmatic signature for Li enrichment. *Lithos* 452-453: 107195.

Rodríguez Fernández LR, Oliveira JT. 2014. Mapa geológico de España y Portugal 1/1.000.000. Cartografía del Instituto Geológico y Minero de España, Geological and Mining Institute of Spain (IMGE) and the National Laboratory of Energy and Geology (LNGE, Portugal).

Romer RL, Pichavant M. 2021. Rare metal granites and pegmatites. In: Encyclopedia of geology, 2nd ed. Vol. 5, pp. 840–846.

Shaw RA, Goodenough KM, Roberts NMW, Horstwood MSA, Chenery SR., Gunn AG. 2016. Petrogenesis of rare-metal pegmatites in high-grade metamorphic terranes: a case study from the lewisian gneiss complex of north-west Scotland. *Precambrian Res* 281: 338–362.

Simons B, Shail RK, Andersen JCØ. 2016. The petrogenesis of the early permian Variscan granites of the Cornubian Batholith: lower plate post-collisional peraluminous magmatism in the rhenohercynian zone of SW England. *Lithos* 260: 76–94.

Sláma J, Košler J, Condon DJ, *et al.* 2008. Plešovice zircon – a new natural reference material for U-Pb and Hf isotopic microanalysis. *Chem Geol* 249: 1–35.

Stacey JS, Kramers JD. 1975. Approximation of terrestrial lead isotope evolution by a two-stage model. *Earth Planet Sci Lett* 26: 207–221.

Stepanov A, Mavrogenes JA, Meffre S, Davidson P. 2014. The key role of mica during igneous concentration of tantalum. *Contrib Mineral Petrol* 167: 1–8.

Stewart DB. 1978. Petrogenesis of lithium-rich pegmatites. *Am Mineral* 63: 970–980.

Tapster S, Bright JWG. 2020. High-precision ID-TIMS cassiterite U-Pb systematics using a low-contamination hydrothermal decomposition: implications for LA-ICP-MS and ore deposit geochronology. *Geochronology* 2: 425–441.

Thomas R, Davidson P. 2012. Water in granite and pegmatite-forming melts. *Ore Geol Rev* 46: 32–46.

Tischendorf G, Gottesmann B, Foerster HJ, Trumbull RB. 1997. On Li-bearing micas: estimating Li from electron microprobe analyses and an improved diagram for raphical representation. *Mineral Mag* 61: 809–834.

Van Lichtervelde M, Grand'Homme A, de Saint-Blanquat M, Olivier P, Gerdes A, Paquette JL, *et al.* 2017. U-Pb geochronology on zircon and columbite-group minerals of the Cap de Creus pegmatites, NE Spain. *Mineral Petrol* 111: 1–21.

Van Lichtervelde M, Holtz F, Melcher F. 2018. The effect of disequilibrium crystallization on Nb-Ta fractionation in pegmatites: constraints from crystallization experiments of tantalite-tapiolite. *Am Mineral* 103: 1401–1416.

Vermeesch P. 2018. IsoplotR: a free and open tool box for geochronology. *Geosci Front* 9: 1479–1493.

Vieira R. 2010. Aplitopegmatitos com elementos raros da região entre Almendra (VN de Foz Côa) e Barca d'Alva (Figueira de Castelo Rodrigo). Campo aplitopegmatítico da Fregeneda-Almendra. PhD Thesis. Faculdade de Ciências da Universidade do Porto.

Vieira R, Roda-Robles E, Pesquera A, Lima A. 2011. Chemical variation and significance of micas from the Fregeneda-Almendra pegmatitic field (Central-Iberian Zone, Spain and Portugal). *Am Mineral* 96: 637–645.

Villar P, Fernández Ruíz J, Bellido Mulas F, Sanz Santos MA, Carrasco RM, Rodríguez Fernández LR. 1990. Mapa Geológico de España. Escala 1:50.000. Lumbrales. 474–475. Instituto Tecnológico GeoMinero de España.

Villaros A, Pichavant M. 2019. Mica-liquid trace elements partitioning and the granite-pegmatite connection: the St-Sylvestre complex (Western French Massif Central). *Chem Geol* 528: 119265.

Whitney DL, Evans BW. 2010. Abbreviations for names of rock-forming minerals. *Am Mineral* 95: 185–187.

Wise MA, Francis CA, Černý P. 2012. Compositional and structural variations in columbite-group minerals from granitic pegmatites of the Brunswick and Oxford fields, Maine: Differential trends in F-poor and F-rich environments. *Can Mineral* 50: 1515–1530.

Zhang DL, Peng JT, Hu RZ, Yuan SD, Zheng DS. 2011. The closure of U-Pb isotope system in cassiterite and its reliability for dating. *Geol Rev* 57: 549–554.

Zhang D, Peng J, Coulson IM, Hou L, Li S. 2014. Cassiterite U-Pb and muscovite ^{40}Ar-^{39}Ar age constraints on the timing of mineralization in the Xuebaoding Sn-W-Be deposit, western China. *Ore Geol Rev* 62: 315–322.

Cite this article as: Ballouard C, Carr P, Parisot F, Gloaguen É, Melleton J, Cauzid J, Lecomte A, Rouer O, Salsi L, Mercadier J. 2024. Petrogenesis and tectonic-magmatic context of emplacement of lepidolite and petalite pegmatites from the Fregeneda-Almendra field (Variscan Central Iberian Zone): clues from Nb-Ta-Sn oxide U-Pb geochronology and mineral geochemistry, *BSGF - Earth Sciences Bulletin* **195**: 3.